Fermilab

FERMILAB-Pub-02/134-T July 2002

RMU-SEMS-011002
NIKHEF/2002-005
ITP-2002/29
FERMILAB-Pub-02/134-T
UPRF-2002-10

The fully differential single-top-quark cross section in next-to-leading order QCD

B. W. Harris[a], E. Laenen[b,c], L. Phaf[b], Z. Sullivan[d], S. Weinzierl[e]

[a] *Robert Morris University, Coraopolis, PA 15108, USA*

[b] *NIKHEF, P.O. Box 41882, NL-1009 DB, Amsterdam, The Netherlands*

[c] *Institute for Theoretical Physics, Utrecht University, Utrecht, The Netherlands*

[d] *Theoretical Physics Department, Fermi National Accelerator Laboratory, Batavia, IL 60510-0500, USA*

[e] *Dipartimento di Fisica, Università di Parma, INFN Gruppo Collegato di Parma, 43100 Parma, Italy*

(July 3, 2002)

Abstract

We present a new next-to-leading order calculation for fully differential single-top-quark final states. The calculation is performed using phase space slicing and dipole subtraction methods. The results of the methods are found to be in agreement. The dipole subtraction method calculation retains the full spin dependence of the final state particles. We show a few numerical results to illustrate the utility and consistency of the resulting computer implementations.

1 Introduction

Single-top-quark production provides an excellent opportunity to study the charged-current weak-interaction of the top quark [1–8]. Measurement of the production cross section of single top quarks is planned at both the Fermilab Tevatron and the CERN Large Hadron Collider (LHC) [9]. The D0 [10] and CDF [11] collaborations have already set limits on both the s-channel and t-channel cross sections using data collected during run I of the Fermilab Tevatron, and have developed strategies for discovery at the current run II.

Within the standard model, the single-top-quark cross section allows a direct measurement of the Cabibbo-Kobayashi-Maskawa (CKM) matrix element V_{tb}. Further, the short lifetime of the top quark presents an opportunity to observe the polarization of the top quark at production, and hence directly probe the $V-A$ nature of the weak interaction [12, 13].

Further, the mass of the top quark is comparable to the electroweak symmetry breaking scale, which has lead to speculation regarding new physics involving the top quark for some time [14]. There are many proposals to use these measurements to study non-standard couplings [15–23], strong dynamics [24–27], flavor changing neutral currents [28, 29], CP violation [30–32], supersymmetry [33–35], R-parity-violating supersymmetry [36–39], and Kaluza-Klein modes [40].

The characteristics of single-top-quark production form a new class of benchmarks for testing Quantum Chromodynamics (QCD). Experimental comparisons to the calculated kinematic distributions can provide a handle on inputs to the calculation. For instance, this process involves directly the bottom quark parton distribution function. Currently this function is constrained only indirectly though global fits [41–43] to data. The bottom-quark density is then calculated from the light parton densities [44–50] in the context of QCD. Including a process that depends directly on the bottom density into the global analysis would be of great value to LHC observables, as their typical scale will be much larger than the bottom mass where the evolution begins.

Finally, single-top-quark production is a background to all signals with $W+$jet or $W+b$ as backgrounds. This background is significant in a number of Higgs search channels (for a review see [51]) and other new physics, such as R-parity conserving [52] and violating [53,54] supersymmetry searches.

In this paper we present and discuss new calculations of single-top-quark production at next-to-leading order (NLO) in QCD. Earlier calculations of the NLO single-top-quark-production cross sections exist in the literature. The first calculation [55] was for the double differential cross section and used small masses for the gluons and quarks to regularize infrared and collinear divergences. Mass factorization was performed in the Deep Inelastic Scattering (DIS) scheme. Subsequent NLO calculations for the s-channel [56, 57] and t-channel [28, 58] modes used dimensional regularization and expressed the semi-inclusive cross section in terms of the Modified Minimal Subtraction ($\overline{\rm MS}$) factorization scheme. The value of our work is that the results are fully differential (meaning experimental cuts and jet finders can be applied), the results contain spin information, and the results use standard methods and schemes. The calculational methods used are an instructive step

toward the computation of NLO corrections to the $t\bar{b}j$ production channel that should also be considered when studying single-top-quark production.

The NLO cross section receives contributions from virtual corrections and real emission diagrams. Taken separately, both parts are divergent and therefore cannot be evaluated in a straightforward way numerically on a computer. Only the sum of the virtual corrections and the real emission contributions is finite after mass factorization. Writing a general-purpose NLO Monte-Carlo based program therefore requires the analytic cancellation of singularities before any numerical integration can be performed.

The two main general methods to handle the cancellation of singularities without loss of information are the phase space slicing [59–66] and the subtraction [67–74] methods. In this paper we implement the phase space slicing method of one [65] and two [66] cutoffs, and the subtraction-based dipole formalism of Ref. [73]. We find that the results of all methods agree. The dipole calculation uses helicity amplitudes and therefore contains the complete spin correlations of the participating partons.

We organize this paper as follows. In the next section we present an overview of the amplitudes entering the calculation. Section 3 discusses the framework of the phase space slicing method and presents the attendant analytic results. Section 4 discusses the cancellation of divergences within the context of the massive dipole subtraction method, and gives the results for all relevant amplitudes. This Section also contains a detailed discussion of scheme independence for different ways of handling γ_5. The analytic results of Secs. 3 and 4 are presented using different, but self-consistent, notations appropriate to their methods of handling of infrared divergences. Brief numerical results are presented in Sec. 5, along with a comparison of the methods. Our conclusions are followed by an Appendix containing the relevant one-loop scalar integrals.

2 Overview

The lowest-order Feynman diagrams are shown in Fig. 1. They are commonly distinguished by the sign of the W boson momentum squared. The t-channel flavor excitation process

$$u + b \to t + d\,, \tag{1}$$

occurs via the exchange of a virtual space-like W-boson, and the Drell-Yan-like s-channel process

$$u + \bar{d} \to t + \bar{b}\,, \tag{2}$$

occurs via a virtual time-like W-boson. In reaction (1) it is understood that we may replace the (u,d)-quark pair by $(\bar{d},\bar{u})$, (c,s) and $(\bar{s},\bar{c})$. In reaction (2) we may replace the $(u,\bar{d})$-pair by $(c,\bar{s})$. In addition, CKM suppressed combinations are included at all vertices.

For each channel the fully differential spin-averaged Born cross section can be written as

$$d\sigma_p^{(0)} = \frac{1}{2s}\overline{\sum}\,|\mathcal{M}_{p,\mathrm{Born}}|^2\,d\mathrm{PS}_2\,, \tag{3}$$

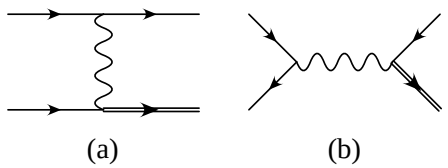

Figure 1: The leading order Feynman diagrams for reactions given in (a) Eq. 1 and (b) Eq. 2. The top quark line is doubled.

where s is the partonic center-of-momentum energy squared, and we use $p = s, t$ to denote the channel. The two body phase space is given by

$$d\mathrm{PS}_2 = \frac{1}{(2\pi)^2}\frac{d^3p_1}{2E_1}\frac{d^3p_2}{2E_2}\delta^{(4)}(q - p_1 - p_2)\,. \tag{4}$$

The t-channel Born matrix element squared summed (averaged) over final (initial) state spin and color states is

$$\overline{\sum}\left|\mathcal{M}_{t,\mathrm{Born}}\right|^2 = \frac{1}{4}g^4|V_{ud}|^2|V_{tb}|^2 s(s - m_t^2)\left|\frac{1}{t - M_W^2}\right|^2\,. \tag{5}$$

Here, $s = (p_u + p_b)^2$ and $t = (p_u - p_d)^2$, the partonic reaction sub-energy squared and the square of the momentum transfer across the W, respectively. The CKM matrix elements $|V_{ij}|$ may be changed for the given particles, and m_t is the top-quark mass. The result for the s-channel is obtained by interchanging s and t, and letting $s = (p_u + p_{\bar{d}})^2$ and $t = (p_u - p_{\bar{b}})^2$. In Sec. 4 we discuss the cross section without the sum over spins.

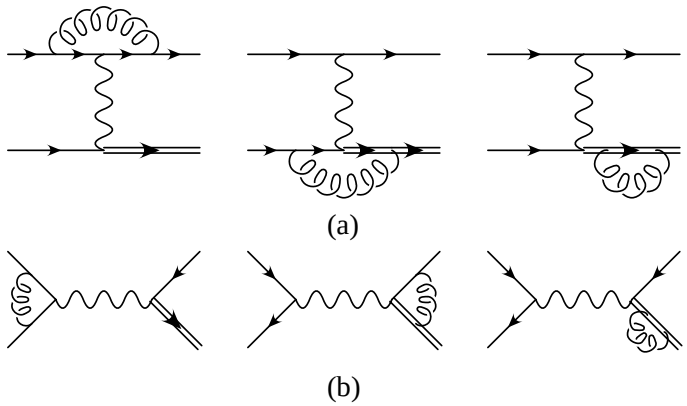

Figure 2: The one-loop virtual corrections to the (a) t-channel and (b) s-channel amplitudes.

At next-to-leading order we must include the virtual QCD corrections to Eqs. (1) and (2), shown in Fig. 2. To obtain the real emission contributions one must attach a gluon in

all possible ways to the diagrams in Fig. 1. The resulting crossed diagrams may be written as

$$
\begin{aligned}
u + \bar{d} &\to t + \bar{b} + g\,, && (6)\\
u + b &\to t + d + g \\
\bar{d} + b &\to t + \bar{u} + g\,, && (7)\\
u + g &\to t + \bar{b} + d \\
\bar{d} + g &\to t + \bar{b} + \bar{u}\,, && (8)\\
g + b &\to t + d + \bar{u}\,. && (9)
\end{aligned}
$$

These crossings may belong either to the s or t channel, and their assignment is governed by the collinear singularity structure. It is useful to distinguish whether the gluon attaches to the fermion current containing the heavy-quark line (h) in Fig. 1 or to the current containing only the light-quark lines (l). Note that the contributions from h and l radiation do not interfere in the cross section due to color conservation [56, 58].

The diagrams in Eq. (6) belong fully to the s-channel, and diagrams in Eq. (7) belong to the t-channel. For crossing in Eq. (8) let us consider the first process $u + g \to t + \bar{b} + d$. In the heavy-quark line the gluon can split into a collinear $b\bar{b}$-pair with reduced process $u + b \to t + d$, so that this crossing belongs to the t-channel. In the light-quark line the gluon can split into a collinear $d\bar{d}$-pair, with reduced process $u + \bar{d} \to t + \bar{b}$, so that this crossing belongs to the s-channel. The classification of the second process in Eq. (8) is similar, with the role of the u- and d-type quarks exchanged. Finally, in Eq. (9), the gluon connected to the light-quark line can split either into a collinear $u\bar{u}$-pair or into a collinear $d\bar{d}$-pair. In both cases the process reduces to the t-channel process $u + b \to t + d$ or $\bar{d} + b \to t + \bar{u}$. Crossing of Eq. (9) to the heavy-quark line is not included in our calculation as it involves on-shell W-decay into light fermions, and is classified as W-top associated production. The cross section for this process is estimated to be negligibly small for the Tevatron [7, 8, 75–77].

In what follows we consider only the production of a single top quark, but the relevant expressions for the production of an antitop quark may easily be obtained by charge conjugation. Our calculational framework is further specified as follows: we set the bottom quark mass to zero, so that we work with 5 massless flavors in the parton distribution functions. It is important to use a consistent set of 5-flavor parton distribution functions, in which the 5-flavor set has been computed from a lower flavor number set via NLO matching conditions [44] that preserve the momentum sum rule. To handle divergences occurring at intermediate stages of the calculation we use dimensional regularization ($D = 4 - 2\epsilon$). Details describing renormalization of the vertices that contain γ_5 are given in Sec. 4.2. Collinear divergences are subtracted in the standard $\overline{\rm MS}$ scheme. We use the Feynman gauge for the gluon propagator.

3 Phase space slicing

In the phase space slicing method a subregion of phase space containing soft and collinear singularities is defined. If the subregion is small enough, one may make simplifying kinematic approximations in the phase space integrals, so that they can be performed analytically. To define the size and shape of this subregion one introduces one or two theoretical cutoff parameters (for common or separate treatment of collinear and soft contributions, respectively). The final cross section should not depend on the choice made for the partitioning. Below we discuss the application of these methods to single-top-quark production.

3.1 Phase space slicing with two cutoffs (δ_s, δ_c)

A detailed description of the phase space slicing method with two cutoffs has recently been given in Ref. [66]. In this section we present the results needed for single-top-quark production. We follow closely the notation of Ref. [66].

In the two cutoff method, phase space is divided into a hard (H) and soft (S) region. The contribution from the latter region is computed by applying the eikonal approximation to the radiative processes in Eqs. (6–9). The soft region of phase space is defined by a condition on the energy of the soft gluon in the partonic center-of-momentum frame:

$$0 \le E_g \le \delta_s \frac{\sqrt{s}}{2}\,. \tag{10}$$

The hard region is then defined by $E_g > \delta_s\sqrt{s}/2$. After performing the D-dimensional angular integrations of the gluon in the region defined in Eq. (10), the soft contribution is found to be

$$d\sigma_p^{(S)} = d\sigma_p^{(0)} \left[\frac{\alpha_s}{2\pi}\frac{\Gamma(1-\epsilon)}{\Gamma(1-2\epsilon)}\left(\frac{4\pi\mu^2}{s}\right)^{\epsilon}\right]\left(\frac{A_2^p}{\epsilon^2}+\frac{A_1^p}{\epsilon}+A_0^p\right), \tag{11}$$

with $p = s, t$ labeling the channel. For the s-channel

$$\begin{aligned}
A_2^s &= 3C_F \\
A_1^s &= C_F\left[1 - 6\ln\delta_s - \ln\left(\frac{s}{m^2}\right)\right] \\
A_0^s &= C_F\Bigg[6\ln^2\delta_s - 2\ln\delta_s + 2\ln\delta_s\ln\left(\frac{s}{m^2}\right) \\
&+ \frac{s+m^2}{s-m^2}\ln\left(\frac{s}{m^2}\right) - 2\mathrm{Li}_2(\beta) - \frac{1}{2}\ln^2\left(\frac{s}{m^2}\right)\Bigg],
\end{aligned} \tag{12}$$

and for the t-channel

$$\begin{aligned}
A_2^t &= 3C_F \\
A_1^t &= C_F\left[1 - 6\ln\delta_s - 2\ln\left(\frac{-t}{s\beta}\right) - \ln\left(\frac{(m^2-t)^2}{m^2 s}\right)\right]
\end{aligned}$$

$$
\begin{aligned}
A_0^t &= C_F\Bigg[6\ln^2\delta_s - 2\ln\delta_s + 4\ln\delta_s\ln\left(\frac{-t}{s\beta}\right) \\
&\quad +2\ln\delta_s\ln\left(\frac{(m^2-t)^2}{m^2 s}\right) + \frac{s+m^2}{s-m^2}\ln\left(\frac{s}{m^2}\right) + \ln^2\left(\frac{-t}{s\beta}\right) + 2\mathrm{Li}_2\left(1+\frac{t}{s\beta}\right) \\
&\quad -\frac{1}{2}\ln^2\left(\frac{s}{m^2}\right) + \ln^2\left(\frac{m^2}{m^2-t}\right) + 2\mathrm{Li}_2\left(\frac{t}{m^2}\right) - 2\mathrm{Li}_2\left(\frac{u}{s+u}\right)\Bigg], \qquad (13)
\end{aligned}
$$

where the top-quark mass is denoted as m, and $\beta = 1 - m^2/s$.

The hard region is further divided into hard collinear (HC) and hard-noncollinear ($\mathrm{H}\overline{\mathrm{C}}$) regions. The latter is computed in 4 dimensions, integrating numerically over the $\mathrm{H}\overline{\mathrm{C}}$ phase space using standard Monte Carlo methods. The HC contributions arise from integration over those regions of phase space where any invariant, $s_{ij} = (p_i + p_j)^2$ or $t_{ij} = (p_i - p_j)^2$, appearing in the denominator becomes smaller in magnitude than $\delta_c s$. The singular regions are distinguished by whether they come from initial or final state radiation. The latter are given by

$$
d\sigma_p^{(HC,FS)} = d\sigma_p^{(0)}\left[\frac{\alpha_s}{2\pi}\frac{\Gamma(1-\epsilon)}{\Gamma(1-2\epsilon)}\left(\frac{4\pi\mu^2}{s}\right)^{\epsilon}\right]\left(\frac{A_1}{\epsilon} + A_0\right), \qquad (14)
$$

with

$$
\begin{aligned}
A_1 &= C_F\left(2\ln\delta_s + \frac{3}{2} - 2\ln\beta\right) \\
A_0 &= C_F\Bigg[\frac{7}{2} - \frac{\pi^2}{3} - \ln^2\delta_s - \ln^2\beta + 2\ln\delta_s\ln\beta \\
&\quad - \ln\delta_c\left(2\ln\delta_s + \frac{3}{2} - 2\ln\beta\right)\Bigg], \qquad (15)
\end{aligned}
$$

for both channels (all massless partons in the Born cross sections are fermions).

The collinear contributions from the initial state are given by the sum of two contributions. The first is the finite remainder after mass factorization. The second results from a mismatch in integration limits when subtracting the mass factorization counter-term.

$$
d\sigma_{p,C}^{ij\to FS} = d\sigma_p^{(0)}\left[\frac{\alpha_s}{2\pi}\frac{\Gamma(1-\epsilon)}{\Gamma(1-2\epsilon)}\left(\frac{4\pi\mu^2}{s}\right)^{\epsilon}\right]\left[\widetilde{f}_j^H(z,\mu_F) + \left(\frac{A_1^{sc}}{\epsilon} + A_0^{sc}\right) f_j^H(z,\mu_F)\right]. \qquad (16)
$$

The modified parton distribution function $\widetilde{f}$ is given in Ref. [66]. For the reaction at hand we only need consider the quark-quark initial state splitting, so

$$
\begin{aligned}
A_1^{sc} &= C_F\left(2\ln\delta_s + \frac{3}{2}\right) \\
A_0^{sc} &= C_F\left(2\ln\delta_s + \frac{3}{2}\right)\ln\left(\frac{s}{\mu_F^2}\right). \qquad (17)
\end{aligned}
$$

The virtual contribution is obtained as explained in the Secs. 4.1 and 4.2. The results in the notation of this section are

$$
d\sigma_p^{(V)} = d\sigma_p^{(0)}\left[\frac{\alpha_s}{2\pi}\frac{\Gamma(1-\epsilon)}{\Gamma(1-2\epsilon)}\left(\frac{4\pi\mu^2}{s}\right)^{\epsilon}\right]\left(\frac{A_2^V}{\epsilon^2} + \frac{A_1^V}{\epsilon} + A_0^V\right) + \left(\frac{\alpha_s}{2\pi}\right)d\tilde{\sigma}_p^{(V)}, \qquad (18)
$$

where

$$
\begin{aligned}
A_2^V &= C_F \left\{ [-2] - [1] \right\} \\
A_1^V &= C_F \left\{ \left[-3 - 2\ln\left(\frac{s}{-q^2}\right) \right] + \left[-\frac{5}{2} - 2\ln(1-\lambda) - \ln\left(\frac{s}{m^2}\right) \right] \right\} \\
A_0^V &= C_F \left\{ \left[-\ln^2\left(\frac{s}{-q^2}\right) - 3\ln\left(\frac{s}{-q^2}\right) - 8 - \frac{\pi^2}{3} \right] \right. \\
&+ \left[-\frac{1}{2}\ln^2\left(\frac{s}{m^2}\right) - \frac{5}{2}\ln\left(\frac{s}{m^2}\right) - 2\ln(1-\lambda)\ln\left(\frac{s}{m^2}\right) - 6 \right. \\
&- \left. \left. \frac{1}{\lambda}\ln(1-\lambda) - \ln^2(1-\lambda) - 2\ln(1-\lambda) + 2\mathrm{Li}_2(\lambda) - \frac{\pi^2}{3} \right] \right\} . \qquad (19)
\end{aligned}
$$

In the above we have defined $\lambda \equiv q^2/(q^2 - m^2)$. Further, the separate terms in the square brackets originate from the massless-massless or the massive-massless vertex corrections. For the t-channel one sets $q^2 = t$, while for the s-channel one sets $q^2 = s$.

$$
d\tilde{\sigma}_t^{(V)} = \frac{1}{2s}\frac{1}{4} g^4 |V_{ud}|^2 |V_{tb}|^2 C_F \frac{m^2 s u}{t} \ln\left(\frac{m^2}{m^2 - t}\right) \left(\frac{1}{t - M_W^2}\right)^2 d\Gamma_2 , \qquad (20)
$$

is the t-channel finite piece in the virtual contribution that is not proportional to the Born cross section. It results from the interference of the renormalized massive-massless vertex with the Born amplitude. The s-channel version may be obtained by crossing.

At this point one can see that the two body weight is finite: $A_2^p + A_2^V = 0$ and $A_1^p + A_1^V + A_1 + 2A_1^{sc} = 0$. The factor of two occurs since there are two quark legs, either of which can emit a gluon. The final finite two-body cross section is given by the sum of the residual $\widetilde{f}$ terms from both the quark-quark and quark-gluon initiated processes and the finite two-body weights. The result, summed over parton flavors is

$$
\begin{aligned}
\sigma^{(2)} &= \left(\frac{\alpha_s}{2\pi}\right) \sum_{a,b} \int dx_1 dx_2 \left\{ f_a^{H_1}(x_1,\mu_F) f_b^{H_2}(x_2,\mu_F) \left[d\sigma_p^{(0)} \left(A_0^p + A_0^V + A_0 + 2A_0^{sc} \right) + d\tilde{\sigma}_p^{(V)} \right] \right. \\
&+ \left. d\sigma_p^{(0)} \left[f_a^{H_1}(x_1,\mu_F) \widetilde{f}_b^{H_2}(x_2,\mu_F) + \widetilde{f}_a^{H_1}(x_1,\mu_F) f_b^{H_2}(x_2,\mu_F) \right] + (x_1 \leftrightarrow x_2) \right\} . \qquad (21)
\end{aligned}
$$

The three-body contribution is given by

$$
\sigma^{(3)} = \sum_{a,b} \int dx_1 dx_2 \frac{1}{2s} \int_{H\overline{C}} \overline{\sum} |M_3^{(ab)}|^2 d\Gamma_3 , \qquad (22)
$$

with

$$
\overline{\sum} |M_3^{(ab)}|^2 = -\pi g^4 |V_{ud}|^2 |V_{tb}|^2 \Psi_i \quad , i = 1 - 3 . \qquad (23)
$$

The Ψ_i contain the luminosity and Dirac algebra of Eqs. (7–9). We choose initial-state momenta as incoming, and label the momenta for the t-channel as

$$
\begin{aligned}
\Psi_1 : u(p_1) b(p_2) &\rightarrow d(p_3) t(p_4) g(p_5) , \qquad (24) \\
\Psi_2 : u(p_1) g(p_2) &\rightarrow d(p_3) t(p_4) \bar{b}(p_5) , \qquad (25) \\
\Psi_3 : g(p_1) b(p_2) &\rightarrow d(p_3) t(p_4) \bar{u}(p_5) . \qquad (26)
\end{aligned}
$$

The t-channel Ψ_i are given by

$$\begin{aligned}
\Psi_1 &= 2C_F F_1 \left(\frac{s_{12}\left(t'_{14}-s'_{34}\right)-s'_{34}t_{25}}{t_{15}} - \frac{s_{12}\left(s'_{34}+s'_{45}\right)-s'_{34}t_{23}}{s_{35}} \right. \\
&\qquad \left. - \frac{t_{13}\left[s_{12}\left(2s'_{34}+s'_{45}\right)+s'_{34}t_{25}\right]}{t_{15}s_{35}} \right) \\
&\quad +2C_F F_2 \left(\frac{s_{12}\left(t_{23}-s'_{34}\right)-s'_{34}t_{15}}{t_{25}} - \frac{s_{12}\left(s'_{34}+s_{35}\right)\left(1-2m_t^2/s'_{45}\right)-s'_{34}t'_{14}}{s'_{45}} \right. \\
&\qquad \left. - \frac{t'_{24}\left[s_{12}\left(2s'_{34}+s_{35}\right)+s'_{34}t_{15}\right]}{t_{25}s'_{45}} \right) , \qquad (27) \\
\Psi_2 &= F_2 \left(\frac{s_{12}s'_{34}+t_{15}\left(s'_{34}-s_{35}\right)}{t_{25}} + \frac{t_{15}\left(s'_{34}+t_{23}\right)\left(1-2m_t^2/t'_{24}\right)-s'_{34}t'_{14}}{t'_{24}} \right. \\
&\qquad \left. + \frac{s'_{45}\left[s_{12}s'_{34}+t_{15}\left(t_{23}+2s'_{34}\right)\right]}{t'_{24}t_{25}} \right) , \qquad (28) \\
\Psi_3 &= F_1 \left(\frac{s_{12}s'_{34}+t_{25}\left(s'_{34}-s'_{45}\right)}{t_{15}} + \frac{t_{25}\left(s'_{34}+t'_{14}\right)-s'_{34}t_{23}}{t_{13}} \right. \\
&\qquad \left. + \frac{s_{35}\left[s_{12}s'_{34}+t_{25}\left(t'_{14}+2s'_{34}\right)\right]}{t_{13}t_{15}} \right) , \qquad (29)
\end{aligned}$$

where $C_F = 4/3$, $s_{ij} = (p_i + p_j)^2$, $t_{ij} = (p_i - p_j)^2$, $s'_{ij} = s_{ij} - m_t^2$, $t'_{ij} = t_{ij} - m_t^2$,

$$F_1 = \frac{\alpha_{s\,l}}{\left(t_{24}-M_W^2\right)^2} L_l \, , \qquad (30)$$

$$F_2 = \frac{\alpha_{s\,h}}{\left(t_{13}-M_W^2\right)^2} L_h \, , \qquad (31)$$

$\alpha_{s\,l(h)}$ and the luminosity functions $L_{l(h)} = f_a^{H_1}(x_1, \mu_{F\,l(h)}) f_b^{H_2}(x_2, \mu_{F\,l(h)})$ are evaluated using the scales at the light(heavy)-quark lines, respectively. All other s- and t-channel matrix elements can be obtained by crossing. Physical predictions follow from the sum $\sigma^{(2)} + \sigma^{(3)}$, which is cutoff independent for sufficiently small cutoffs as shown below.

3.2 Phase space slicing with one cutoff ($s_{\min}$)

The calculation using the one cutoff slicing method is similar to the one using the two cutoff slicing method, with some differences that we now address. In this method, a pair of partons with momenta p_i and p_j is defined to be unresolved if

$$|2p_i \cdot p_j| < s_{\min} \, , \qquad (32)$$

with $s_{\min}$ small compared to the hard scale of the process. The condition in Eq. (32) can occur if either p_i and p_j are collinear, or if one of the two is soft. This method, combined with the use of color-decomposed amplitudes and universal crossing functions,

has been developed into a general method for computing with minimal calculational effort fully differential NLO production cross sections of bosons and jets in [63,64] and identified hadrons and heavy quarks in [65]. The single-top-quark production process has a relatively simple color structure, so we do not need to decompose the scattering amplitudes into color-ordered subamplitudes.

The treatment of the virtual corrections is no different from the two cutoff method. To determine the radiative corrections, all partons are first crossed to the final state, and resolved and unresolved contributions are identified according to the criterion in Eq. (32). The unresolved contributions, (soft and collinear) can be found in [63–65] expressed in $D = 4 - 2\epsilon$ dimensions. The soft contributions are expressed in terms of the momenta for partons in lowest order kinematics with all partons in the final state

$$0 \to \bar{u} + d + t + \bar{b}\,, \tag{33}$$

and are given by

$$d\sigma^{(S)} = d\sigma^{(0)} \left[\frac{\alpha_s\, C_F}{\pi} \frac{1}{\Gamma(1-\epsilon)} \left(\frac{4\pi\mu^2}{s_{\rm min}}\right)^{\epsilon}\right] \left[\frac{1}{\epsilon^2}\left(\frac{2p_u\cdot p_d}{s_{\rm min}}\right)^{\epsilon} + \mathcal{J}(m,0)\left(\frac{2p_t\cdot p_b}{s_{\rm min}}\right)^{\epsilon}\right]\,, \tag{34}$$

with $d\sigma^{(0)}$ obtained by crossing all momenta to the final state, and

$$\begin{aligned}
&1)\;\; 2p_t\cdot p_b \geq m^2 \;:\quad \mathcal{J}(m,0) \;=\; \frac{1}{\epsilon^2} - \frac{1}{2\epsilon^2}\left(\frac{2p_t\cdot p_b}{m^2}\right)^{\epsilon} + \frac{1}{2\epsilon}\left(\frac{2p_t\cdot p_b}{m^2}\right)^{\epsilon} - \frac{\pi^2}{12} + \frac{m^2}{2p_t\cdot p_b} \\
&2)\;\; 2p_t\cdot p_b \leq m^2 \;:\quad \mathcal{J}(m,0) \;=\; \left(\frac{2p_t\cdot p_b}{m^2}\right)^{-\epsilon}\left(\frac{1}{2\epsilon^2} + \frac{1}{2\epsilon} - \frac{\pi^2}{12} + 1\right)\,.
\end{aligned} \tag{35}$$

The s-channel contribution is then obtained by replacing $2p_u\cdot p_d \to s$, $2p_t\cdot p_b \to s - m^2$. The t-channel contribution is obtained by replacing $2p_u\cdot p_d \to t$, $2p_t\cdot p_b \to t - m^2$, which leads to π^2 terms after expanding in ϵ. The collinear contributions are likewise given by

$$\begin{aligned}
d\sigma^{(C)} \;=\; & -d\sigma^{(0)}\left[\frac{\alpha_s\, C_F}{\pi}\frac{1}{\Gamma(1-\epsilon)}\left(\frac{4\pi\mu^2}{s_{\rm min}}\right)^{\epsilon}\right]\frac{1}{\epsilon} \\
& \times\left[I_{q\to qg}\left(0,\frac{s_{\rm min}}{2p_u\cdot p_d}\right) + I_{\bar{q}\to qg}\left(\frac{s_{\rm min}}{2p_u\cdot p_d},0\right) + I_{\bar{q}\to qg}\left(\frac{s_{\rm min}}{2p_t\cdot p_b},0\right)\right]\,.
\end{aligned} \tag{36}$$

The I functions are given in Refs. [63, 64]. The s-channel contribution is obtained by replacing $2p_u\cdot p_d \to s$, $2p_t\cdot p_b \to s - m^2$. The t-channel contribution is obtained by replacing $2p_u\cdot p_d \to t$, $2p_t\cdot p_b \to t - m^2$. The sum of these contributions is already finite. One now generates the various subprocesses of single-top-quark production by crossing pairs of partons back to the initial state. Crossing symmetry is not a property of next-to-leading order cross sections, but it may be implemented in the following way.

In general a NLO fully differential cross section for a process with initial hadrons H_1 and H_2 may be written as

$$d\sigma_{H_1\,H_2} = \sum_{a,b}\int dx_1 \int dx_2\, \mathcal{F}_a^{H_1}(x_1)\,\mathcal{F}_b^{H_2}(x_2) d\sigma_{ab}^{NLO}(x_1,x_2)\,, \tag{37}$$

where a, b denote parton flavors and x_1, x_2 are parton momentum fractions. The function $d\sigma_{ab}^{NLO}$ is computed with all-partons-in-the-final-state matrix elements, in which partons a and b have simply been crossed to the initial state, i.e. in which their momenta p_a and p_b have been replaced by $-p_a$ and $-p_b$ (this function does include the π^2 terms resulting from this replacement in the one-loop virtual graphs). The functions $\mathcal{F}_a^H(x)$ are modifications of the parton distribution functions $f_a^H(x, \mu_F)$

$$\mathcal{F}_a^H(x) = f_a^H(x, \mu_F) + \alpha_s C_a^H(x, \mu_F) + O(\alpha_s^2), \tag{38}$$

where $C_a^H(x, \mu_F)$ are finite, universal "crossing functions" [64]. They implement the crossing property for the unresolved contributions, and are given by

$$C_a^{H,\overline{\rm MS}}(x, \mu_F) = \frac{N_C}{2\pi}\left[A_a^H(x, \mu_F)\ln\left(\frac{s_{\rm min}}{\mu_F^2}\right) + B_a^{H,\overline{\rm MS}}(x, \mu_F)\right]. \tag{39}$$

The functions A_a^H, B_a^H functions for the proton are given in [64]. In the unresolved contribution one may simply cross pairs of partons without further modifications.

The full NLO differential cross section can now be written as:

$$\begin{aligned} d\sigma_{H_1 H_2} &= \sum_{a,b}\int dx_1 dx_2 f_a^{H_1}(x_1, \mu_F)\, f_b^{H_2}(x_2, \mu_F)\left[d\sigma_{ab}^{NLO}(x_1, x_2) + \alpha_s(\mu_F)\right. \\ &\left.\times\Big(C_a^{H_1}(x_1, \mu_F) f_b^{H_2}(x_2, \mu_F) + f_a^{H_1}(x_1, \mu_F) C_b^{H_2}(x_2, \mu_F)\Big) d\sigma_{ab}^{LO}(x_1, x_2)\right]. \end{aligned} \tag{40}$$

The unresolved contribution, now including the crossing functions, depends analytically on $s_{\rm min}$, but this $s_{\rm min}$ dependence cancels against that of the resolved contribution. The results produced with this method agree with those of the previous section. In this paper we limit ourselves to some illustrative numerical studies, so that we only employ the dipole and two-cutoff slicing methods for numerical results.

4 Massive Dipole Subtraction Calculation

Within the dipole formalism the NLO cross section is rewritten as

$$\begin{aligned} \sigma^{NLO} &= \int_{n+1} d\sigma^R + \int_n d\sigma^V \\ &= \int_{n+1}\Big(d\sigma^R - d\sigma^A\Big) + \int_n\left(d\sigma^V + \int_1 d\sigma^A\right). \end{aligned} \tag{41}$$

In the second line an approximation term $d\sigma^A$ has been added and subtracted. This is valid if all singularities occur in the final state. For initial state partons there are slight modifications. The approximation $d\sigma^A$ has to fulfill the requirement that $d\sigma^A$ is a proper approximation of $d\sigma^R$ such as to have the same point-wise singular behavior (in

D dimensions) as $d\sigma^R$ itself. Thus, $d\sigma^A$ acts as a local counter-term for $d\sigma^R$ and one can safely perform the limit $\varepsilon \to 0$. This defines a cross-section contribution

$$\sigma^{NLO}_{\{n+1\}} = \int_{n+1} \left(d\sigma^R \Big|_{\varepsilon=0} - d\sigma^A \Big|_{\varepsilon=0} \right) . \tag{42}$$

$d\sigma^A$ is analytically integrable (in D dimensions) over the one-parton subspace leading to soft and collinear divergences. This gives the contribution

$$\sigma^{NLO}_{\{n\}} = \int_{n} \left(d\sigma^V + \int_{1} d\sigma^A \right)_{\varepsilon=0} . \tag{43}$$

The final structure of an NLO calculation is then

$$\sigma^{NLO} = \sigma^{NLO}_{\{n+1\}} + \sigma^{NLO}_{\{n\}} . \tag{44}$$

Since both contributions on the right hand side of Eq. (44) are now finite, they can be evaluated with numerical methods. The $(n+1)$ matrix element is approximated by a sum of dipole terms

$$\begin{aligned} d\sigma^A &\sim \sum_{\text{pairs } i,j} \sum_{k \neq i,j} \mathcal{D}_{ij,k} \\ &= \sum_{\text{pairs } i,j} \sum_{k \neq i,j} -\frac{1}{2p_i \cdot p_j} \langle 1, ..., (\tilde{ij}), ..., \tilde{k}, ... | \frac{\mathbf{T}_k \cdot \mathbf{T}_{ij}}{\mathbf{T}^2_{ij}} V_{ij,k} | 1, ..., (\tilde{ij}), ..., \tilde{k}, ... \rangle , \end{aligned} \tag{45}$$

where the emitter parton is denoted by $\tilde{ij}$ and the spectator by $\tilde{k}$. Here $\mathbf{T}_i$ denotes the color charge operator [72] for parton i and $V_{ij,k}$ is a matrix in the helicity space of the emitter with the correct soft and collinear behavior. $|1, ..., (\tilde{ij}), ..., \tilde{k}, ...\rangle$ is a vector in color- and helicity space. By subtracting from the real emission part the fake contribution we obtain

$$\begin{aligned} d\sigma^R - d\sigma^A = d\phi_{n+1} \Bigg(& |M(p_1, ..., p_{n+1})|^2 \theta^{cut}_{n+1}(p_1, ..., p_{n+1}) \\ & - \sum_{\text{pairs } i,j} \sum_{k \neq i,j} \mathcal{D}_{ij,k}(p_1, ..., p_{n+1}) \theta^{cut}_n(p_1, ..., \tilde{p}_{ij}, ..., \tilde{p}_k, ..., p_{n+1}) \Bigg) . \end{aligned} \tag{46}$$

Both $d\sigma^R$ and $d\sigma^A$ are integrated over the same $(n+1)$ parton phase space, but it should be noted that $d\sigma^R$ is proportional to θ^{cut}_{n+1}, whereas $d\sigma^A$ is proportional to θ^{cut}_n. Here θ^{cut}_n denotes the jet-defining function for n-partons.

The subtraction term can be integrated over the one-parton phase space to yield the term

$$\mathbf{I} \otimes d\sigma^B = \int_1 d\sigma^A = \sum_{\text{pairs } i,j} \sum_{k \neq i,j} \int d\phi_{dipole} \mathcal{D}_{ij,k} . \tag{47}$$

The universal factor $\mathbf{I}$ still contains color correlations, but does not depend on the unresolved parton j. The term $\mathbf{I} \otimes d\sigma^B$ lives on the phase space of the n-parton configuration and has the appropriate singularity structure to cancel the infrared divergences coming from the one-loop amplitude. Therefore,

$$d\sigma^V + \mathbf{I} \otimes d\sigma^B \tag{48}$$

is infrared finite and can easily be integrated by Monte Carlo methods. The explicit forms of the dipole terms $\mathcal{D}_{ij,k}$, together with the integrated counterparts, can be found in Ref. [72] (the original massless case) and in Ref. [73] (extension to massive fermions).

4.1 Calculation of the amplitudes

We have performed three different calculations of the loop amplitudes. One calculation was done using the standard approach in the 't Hooft-Veltman scheme. The second calculation involved treating the γ_5 as anti-commuting in D dimensions, thereby retaining Ward identities for the charged current vertex. In the third one we calculated helicity amplitudes using a four-dimensional scheme. The effects of different prescriptions for γ_5 are discussed more extensively in Sec. 4.2. The results of the three calculations agree with each other, in the sense that they can be related to each other through process-independent finite renormalizations. In addition, we find agreement with the earlier calculations of Refs. [78, 79]. We present here the helicity amplitudes obtained with the third approach. They are more compact and contain the complete spin information. In the standard approach one just calculates the interference between the loop amplitude and the Born term and sums over all spins.

We first list our conventions (for reviews of spinor helicity methods see e.g. [80, 81]). With spinor helicity methods we can express scattering amplitudes in terms of massless Weyl spinors of helicity $\pm\frac{1}{2}$,

$$u(p,\pm) = v(p,\mp) = |p\pm\rangle\,, \qquad \bar{u}(p,\pm) = \bar{v}(p,\mp) = \langle p\pm|\,. \tag{49}$$

External fermion states are directly expressed in terms of these. Our convention is to take all particles outgoing. For example, an outgoing massless fermion with positive helicity is denoted by $\langle p+|$, while an outgoing massless anti-fermion with positive helicity is denoted by $|p-\rangle$. The gluon polarization vectors, of helicity ± 1, may be written as

$$\varepsilon^+_\mu(k,q) = \frac{\langle q-|\gamma_\mu|k-\rangle}{\sqrt{2}\langle qk\rangle}, \qquad \varepsilon^-_\mu(k,q) = \frac{\langle q+|\gamma_\mu|k+\rangle}{\sqrt{2}[kq]}. \tag{50}$$

We use the customary short-hand notation:

$$\langle ij\rangle = \langle p_i - |p_j+\rangle, \qquad [ij] = \langle p_i + |p_j-\rangle. \tag{51}$$

In Eq. (50) k is the gluon momentum and q an arbitrary light-like "reference momentum". The dependence on the choice of q drops out in gauge-invariant amplitudes. We shall also

employ the abbreviations

$$\begin{aligned} \langle i - |k+l|j- \rangle &= \langle ik \rangle [kj] + \langle il \rangle [lj], \\ s_{ij...k} &= (p_i + p_j + ... + p_k)^2 , \end{aligned} \tag{52}$$

with all momenta null-vectors.

To treat the massive top quark within the framework of spinor helicity methods, we use the extension to massive fermions [82–85]. Even though helicity is not a conserved quantum number for a massive particle, a massive positive-energy spinor satisfying the Dirac equation has a two-fold degeneracy (labeled by a spin-component quantized along some axis). With slight abuse of notation we label these two states by "+" and "−". Let p be a four-vector with $p^2 = m^2$ and $p_0 > 0$, and let q be an arbitrary null vector with $q_0 > 0$. We define

$$\begin{aligned} u(p,+) &= \frac{1}{\sqrt{2pq}} (\not{p} + m) |q-\rangle, \qquad v(p,+) = \frac{1}{\sqrt{2pq}} (\not{p} - m) |q-\rangle, \\ u(p,-) &= \frac{1}{\sqrt{2pq}} (\not{p} + m) |q+\rangle, \qquad v(p,-) = \frac{1}{\sqrt{2pq}} (\not{p} - m) |q+\rangle. \end{aligned} \tag{53}$$

For the conjugate spinors we have

$$\begin{aligned} \bar{u}(p,+) &= \frac{1}{\sqrt{2pq}} \langle q- | (\not{p} + m) , \qquad \bar{v}(p,+) = \frac{1}{\sqrt{2pq}} \langle q- | (\not{p} - m) , \\ \bar{u}(p,-) &= \frac{1}{\sqrt{2pq}} \langle q+ | (\not{p} + m) , \qquad \bar{v}(p,-) = \frac{1}{\sqrt{2pq}} \langle q+ | (\not{p} - m) . \end{aligned} \tag{54}$$

It is easy to check that for these spinors the Dirac equations, orthogonality, and completeness relations hold. The dependency on the arbitrary reference momentum q drops out in the final answer.

Given two four-vectors p and q, the spinor product $\langle pq \rangle$ is calculated as follows: If $p_t > 0$ and $q_t > 0$,

$$\langle pq \rangle = \frac{1}{\sqrt{p_+ q_+}} \left(p_\perp q_+ - p_+ q_\perp \right) . \tag{55}$$

Here the light-cone coordinates $p_+ = p_t + p_z$ and $p_\perp = p_x + i p_y$ are used. For negative-energy four-vectors we have

$$\begin{aligned} \langle pq \rangle &= -\langle (-p) q \rangle, \quad \text{for } p_t < 0 , \\ \langle pq \rangle &= -\langle p (-q) \rangle, \quad \text{for } q_t < 0 . \end{aligned} \tag{56}$$

The spinor product $[pq]$ is related to $\langle pq \rangle$ by

$$[pq] = \mathrm{sign}(p_t q_t) \langle qp \rangle^* . \tag{57}$$

We employ amplitudes with all partons outgoing, generating in an economical way the relevant scattering amplitudes by crossing. The lowest-order amplitude is shown in Fig. 1

$$A_{Wb} \;:\; 0 \to t(p_8) + \bar{b}(p_4) + d(p_6) + \bar{u}(p_7)\,, \tag{58}$$

where all momenta are outgoing. We use here the notation of Ref. [86], which explains the unusual labeling of the momenta with p_4, p_6, p_7 and p_8.

Each amplitude we decompose into gauge-invariant partial amplitudes. The color decomposition of the Born amplitude is

$$A_{Wb,born} \;=\; \delta_{84}\delta_{67}A^{[1]}_{Wb,born}\,. \tag{59}$$

It is convenient to factor out some common prefactors from the partial amplitude $A^{[1]}_{Wb,born}$ and to write it as follows:

$$A^{[1]}_{Wb,born} \;=\; \frac{e^2 V_{ud}^* V_{tb}}{2\sin^2\theta_W}\cdot\frac{2i}{s_{67}-m_W^2}\frac{B^{[1]}_{Wb,born}}{\sqrt{-\langle 2-|4+6+7|2-\rangle}}. \tag{60}$$

Here we denote the reference momentum for the massive spinor by $q = p_2$. If one is only interested in the spin-summed squared amplitude, one may choose any arbitrary null vector for p_2, the choices $p_2 = (1,0,0,1)$ or $p_2 = p_6$ are examples. However, by keeping p_2 unspecified, we keep the complete spin information, and our formulas become only slightly more lengthy. The non-vanishing Born amplitudes are

$$\begin{aligned} B^{[1]}_{Wb,born}(p_4^+, p_6^-, p_7^+, p_8^-) &= [47]\langle 6-|4+7|2-\rangle, \\ B^{[1]}_{Wb,born}(p_4^+, p_6^-, p_7^+, p_8^+) &= m\langle 26\rangle[74]. \end{aligned} \tag{61}$$

We now turn our attention to the loop amplitudes. The color decomposition of the one-loop amplitude is given by

$$\begin{aligned} A_{Wb,loop} &= \delta_{67}T^a_{8i}T^a_{i4}A^{[1]}_{Wb,loop} + T^a_{6i}T^a_{i7}\delta_{84}A^{[2]}_{Wb,loop} + T^a_{67}T^a_{84}A^{[3]}_{Wb,loop} \\ &= \frac{N^2-1}{2N}\delta_{67}\delta_{84}A^{[1]}_{Wb,loop} + \frac{N^2-1}{2N}\delta_{67}\delta_{84}A^{[2]}_{Wb,loop} \\ &\quad + \frac{1}{2}\left(\delta_{64}\delta_{87} - \frac{1}{N}\delta_{67}\delta_{84}\right)A^{[3]}_{Wb,loop}. \end{aligned} \tag{62}$$

Here we used the short-hand notation

$$T^a_{84} \;=\; T^a_{i_8 j_4}\,, \tag{63}$$

where a is the color index of the gluon, i_8 is the color index of the quark $t(p_8)$ and j_4 is the color index of the quark $\bar{b}(p_4)$. $A^{[1]}_{Wb,loop}$ corresponds to loop corrections on the t-b line, $A^{[2]}_{Wb,loop}$ to corrections on the u-d line, and $A^{[3]}_{Wb,loop}$ to a gluon exchange between the two lines. Note that we do not have to calculate $A^{[3]}_{Wb,loop}$:

$$2\,\mathrm{Re}\,\left(\delta_{84}\delta_{67}A^{[1]}_{Wb}\right)^* T^a_{67}T^a_{84}A^{[3]}_{Wb,loop} \;=\; 0\,, \tag{64}$$

because the color matrices are traceless. We write

$$
\begin{aligned}
A^{[1]}_{Wb,loop} &= \frac{e^2 V_{ud}^* V_{tb}}{2\sin^2\theta_W}\frac{2i}{s_{67}-m_W^2}\frac{B^{[1]}_{Wb,loop}}{\sqrt{-\langle 2-|4+6+7|2-\rangle}}\frac{g^2}{(4\pi)^2} \\
A^{[2]}_{Wb,loop} &= \frac{e^2 V_{ud}^* V_{tb}}{2\sin^2\theta_W}\frac{2i}{s_{67}-m_W^2}\frac{B^{[2]}_{Wb,loop}}{\sqrt{-\langle 2-|4+6+7|2-\rangle}}\frac{g^2}{(4\pi)^2}\,. \qquad (65)
\end{aligned}
$$

For the helicity configuration $p_4^+, p_6^-, p_7^+, p_8^-$ we obtain

$$
\begin{aligned}
&B^{[1]}_{Wb,loop}(p_4^+, p_6^-, p_7^+, p_8^-) = \\
&\quad 2[47]\Bigg\{\langle 6-|4+7|2-\rangle\langle 4-|6+7|4-\rangle C_0^{(a)}(s_{67},m^2) \\
&\quad +\left[\left(-\frac{1}{2}+\frac{s_{67}}{\langle 4-|6+7|4-\rangle}\right)\langle 6-|4+7|2-\rangle+\frac{1}{2}\frac{s_{467}}{\langle 4-|6+7|4-\rangle}\langle 64\rangle[42]\right]B_0^{(a)}(s_{67},m^2) \\
&\quad -\frac{1}{\langle 4-|6+7|4-\rangle}(s_{67}\langle 6-|4+7|2-\rangle+s_{467}\langle 64\rangle[42])B_0^{(b)}(m^2) \\
&\quad +\frac{1}{2}\frac{\langle 64\rangle[42]}{\langle 4-|6+7|4-\rangle}A_0(m^2)-s_{467}\frac{\langle 64\rangle[42]}{\langle 4-|6+7|4-\rangle}C_0^{(-2\varepsilon)}(s_{67},m^2)\Bigg\} \\
&B^{[2]}_{Wb,loop}(p_4^+, p_6^-, p_7^+, p_8^-) = \\
&\quad -2[47]\langle 6-|4+7|2-\rangle\left(s_{67}C_0^{(b)}(s_{67})+\frac{3}{2}B_0^{(c)}(s_{67})\right). \qquad (66)
\end{aligned}
$$

For the helicity configuration $p_4^+, p_6^-, p_7^+, p_8^+$ we obtain

$$
\begin{aligned}
&B^{[1]}_{Wb,loop}(p_4^+, p_6^-, p_7^+, p_8^+) = \\
&\quad -2m[74]\Bigg[\langle 62\rangle\langle 4-|6+7|4-\rangle C_0^{(a)}(s_{67},m^2) \\
&\quad +\frac{1}{\langle 4-|6+7|4-\rangle}\left(s_{67}\langle 62\rangle-\frac{1}{2}\langle 67\rangle[74]\langle 42\rangle\right)B_0^{(a)}(s_{67},m^2) \\
&\quad -\frac{1}{\langle 4-|6+7|4-\rangle}(s_{67}\langle 62\rangle+\langle 64\rangle\langle 4+|6+7|2+\rangle)B_0^{(b)}(m^2) \\
&\quad +\frac{1}{2}\frac{\langle 64\rangle\langle 4+|6+7|2+\rangle}{s_{467}\langle 4-|6+7|4-\rangle}A_0(m^2)+\frac{\langle 2-|6+7|4-\rangle\langle 46\rangle}{\langle 4-|6+7|4-\rangle}C_0^{(-2\varepsilon)}(s_{67},m^2)\Bigg] \\
&B^{[2]}_{Wb,loop}(p_4^+, p_6^-, p_7^+, p_8^+) = \\
&\quad -2m[74]\langle 26\rangle\left(s_{67}C_0^{(b)}(s_{67})+\frac{3}{2}B_0^{(c)}(s_{67})\right). \qquad (67)
\end{aligned}
$$

The expressions for the standard scalar integrals are collected in the Appendix. The ultraviolet (UV) renormalization is discussed in the next section.

Finally, we need the real emission amplitudes with one additional gluon. These are listed in Eqs. (6–9), and correspond to the process

$$A_{Wg} \quad : \quad 0 \to t(p_8) + \bar{b}(p_4) + g(p_5) + d(p_6) + \bar{u}(p_7)\,. \tag{68}$$

The color decomposition reads

$$A_{Wg,real} \;=\; T^5_{84}\delta_{67}A^{[1]}_{Wg,real} + \delta_{84}T^5_{67}A^{[2]}_{Wg,real}\,. \tag{69}$$

These amplitudes have been calculated in Ref. [86]. For convenience we list them here. We have

$$\begin{aligned}
A^{[1]}_{Wg,real} &= \frac{ge^2V^*_{ud}V_{tb}}{2\sin^2\theta_W}\cdot\frac{(-i)2\sqrt{2}}{s_{67}-m_W^2}\frac{B^{[1]}_{Wg,real}}{\sqrt{-\langle 2-|4+5+6+7|2-\rangle}},\\
A^{[2]}_{Wg,real} &= \frac{ge^2V^*_{ud}V_{tb}}{2\sin^2\theta_W}\cdot\frac{(-i)2\sqrt{2}}{s_{567}-m_W^2}\frac{B^{[2]}_{Wg,real}}{\sqrt{-\langle 2-|4+5+6+7|2-\rangle}}.
\end{aligned} \tag{70}$$

As reference momentum for the massive spinor we have chosen $q = p_2$. The non-vanishing amplitudes are

$$\begin{aligned}
&B^{[1]}_{Wg,real}(p_4^+,p_5^+,p_6^-,p_7^+,p_8^-)\\
&\quad= \frac{\langle 6-|4+5+7|2-\rangle}{\langle 65\rangle}\left(\frac{\langle 6-|4+5|7-\rangle}{\langle 45\rangle}+\frac{[74]\langle 6-|4+7|5-\rangle}{s_{467}-m^2}\right),\\
&B^{[1]}_{Wg,real}(p_4^+,p_5^+,p_6^-,p_7^+,p_8^+)\\
&\quad= -\frac{m\langle 26\rangle}{\langle 65\rangle}\left(\frac{\langle 6-|4+5|7-\rangle}{\langle 45\rangle}+\frac{[74]\langle 6-|4+7|5-\rangle}{s_{467}-m^2}\right),\\
&B^{[1]}_{Wg,real}(p_4^+,p_5^-,p_6^-,p_7^+,p_8^-)\\
&\quad= \frac{[74]}{[54]\,(s_{467}-m^2)}\Big(\langle 5-|4+6+7|2-\rangle[47]\langle 76\rangle + m^2[24]\langle 56\rangle\Big),\\
&B^{[1]}_{Wg,real}(p_4^+,p_5^-,p_6^-,p_7^+,p_8^+)\\
&\quad= -\frac{m}{s_{467}-m^2}\frac{[47]}{[45]}\left(\langle 25\rangle\langle 67\rangle[74]+\langle 56\rangle\langle 2-|5+6+7|4-\rangle\right),
\end{aligned} \tag{71}$$

$$\begin{aligned}
B^{[2]}_{Wg,real}(p_4^+,p_5^+,p_6^-,p_7^+,p_8^-) &= \frac{\langle 6-|4+5+7|2-\rangle\langle 6-|5+7|4-\rangle}{\langle 56\rangle\langle 75\rangle},\\
B^{[2]}_{Wg,real}(p_4^+,p_5^+,p_6^-,p_7^+,p_8^+) &= \frac{m\langle 62\rangle\langle 6-|5+7|4-\rangle}{\langle 56\rangle\langle 75\rangle},\\
B^{[2]}_{Wg,real}(p_4^+,p_5^-,p_6^-,p_7^+,p_8^-) &= \frac{[74]\langle 2+|(4+5+6+7)(5+6)|7-\rangle}{[57][56]},\\
B^{[2]}_{Wg,real}(p_4^+,p_5^-,p_6^-,p_7^+,p_8^+) &= \frac{m[47]\langle 2-|5+6|7-\rangle}{[57][56]}.
\end{aligned} \tag{72}$$

The matrix element squared is given by

$$|A_{Wg,Real}|^2 = \frac{1}{2}N_C(N_C^2-1)\left(\left|A^{[1]}_{Wg,Real}\right|^2+\left|A^{[2]}_{Wg,Real}\right|^2\right) . \tag{73}$$

There are no interference terms between $A^{[1]}_{Wg,Real}$ and $A^{[2]}_{Wg,Real}$.

4.2 Conversion between schemes and scheme independence

The one-loop amplitudes presented in the previous section have been calculated in a four-dimensional scheme. They differ from the corresponding amplitudes in the 't Hooft-Veltman scheme by finite terms. These finite terms are either of ultraviolet (UV) or infrared (IR) origin and result from expressions of the form ε/ε. To obtain the unique and correct result, one proceeds through the following steps:

- The bare one-loop amplitudes may contain UV-divergences. With the help of a specific regularization scheme these divergences are isolated and removed by renormalization. The explicit form of the renormalization depends on the chosen renormalization scheme.

- The specific combination of regularization and renormalization scheme may break certain Ward identities. These Ward identities have to be restored through finite renormalizations. The required finite renormalizations are universal, i.e. they do not depend on the process under consideration. After this step all finite parts of UV-origin are uniquely fixed.

- In addition, QCD amplitudes may contain IR-divergences. Unitarity requires that we employ the same regularization scheme in the phase space integral over the unresolved real emission part as in the one-loop integral.
  Alternatively, since the structure of the IR-divergences is universal, we may derive simple formulas, which relate the finite parts specific to a certain regularization scheme to the ones of another scheme. We can therefore convert a one-loop amplitude calculated in one scheme to the corresponding amplitude calculated in another scheme.

We will discuss the three steps in detail for the case at hand. To start, let us briefly summarize the properties of the 't Hooft-Veltman scheme and the four-dimensional scheme. The 't Hooft-Veltman scheme treats unobserved particles (particles in loops and unresolved partons in the real emission part) in $D = 4 - 2\varepsilon$ dimensions. Observed particles are taken in four dimensions. γ_5 is a four-dimensional object in the t' Hooft-Veltman scheme, anticommuting with the first four Dirac matrices and commuting with the remaining ones.

The four-dimensional scheme is specified in simple terms by the fermion propagators

$$i\frac{\not{p}_{(4)}+m1_{(4)}}{p^2_{(D)}-m^2} . \tag{74}$$

Four-dimensional Dirac-matrices occur in the numerator, whereas D-dimensional quantities occur in the denominator. Two adjacent Dirac-matrices in the numerator are contracted as

$$\not{p}_{(4)}\not{p}_{(4)} = \left(p^2_{(D)} - p^2_{(-2\varepsilon)}\right) \cdot 1_{(4)} \,, \tag{75}$$

which can be interpreted as the statement "D is effectively larger then 4". $p^2_{(D)}$ can cancel a propagator, whereas $p^2_{(-2\varepsilon)}$ will give rise to an integral in $6-2\varepsilon$ dimensions. It should be kept in mind that the specification given here is just a simple prescription relevant to practical calculations. The scheme is rigorously defined in Ref. [87].

$A_{Wb,loop}$ contains ultraviolet and infrared divergences. Ultraviolet divergences are removed after renormalization of the quark fields

$$\psi_{bare} = Z_\psi^{1/2} \psi_{ren} \,. \tag{76}$$

The renormalized amplitude is obtained as

$$A_{Wb,loop,ren} = \left(Z_\psi^{1/2}\right)^4 A_{Wb,loop,bare} \,. \tag{77}$$

We have to renormalize the fields such that the residuum of the propagators is 1. For light quarks the appropriate renormalization constant is 1, due to a cancellation of UV- and IR- divergent parts. In more detail we have

$$\begin{aligned} Z^{1/2}_{\psi,onshell,FD} &= 1 + \frac{1}{2}\frac{g^2}{(4\pi)^2} C_F \left(-\Delta_{UV} + \Delta_{IR}\right), \\ Z^{1/2}_{\psi,onshell,HV} &= 1 + \frac{1}{2}\frac{g^2}{(4\pi)^2} C_F \left(-\Delta_{UV} + 1_{UV} + \Delta_{IR} - 1_{IR}\right), \end{aligned} \tag{78}$$

where $\Delta = 1/\varepsilon - \gamma + \ln 4\pi$. Here we have indicated with a subscript UV or IR the origins of the divergent parts as well as the origin of additional finite terms which arise from a cancellation of $1/\varepsilon$-terms with terms of order ε. For massive quarks we have

$$\begin{aligned} Z^{1/2}_{\psi,onshell,FD} &= 1 + \frac{1}{2}\frac{g^2}{(4\pi)^2} C_F \left(-3\Delta_{UV} - 5 + 3\ln\frac{m^2}{\mu^2}\right) \\ Z^{1/2}_{\psi,onshell,HV} &= 1 + \frac{1}{2}\frac{g^2}{(4\pi)^2} C_F \left(-3\Delta_{UV} + 1_{UV} - 5 + 3\ln\frac{m^2}{\mu^2}\right) . \end{aligned} \tag{79}$$

After renormalization of the quark field we have

$$\begin{aligned} B^{[1]}_{Wb,loop,ren,FD} &= B^{[1]}_{Wb,loop,bare,FD} + \frac{1}{2}\left(-3\Delta - 5 + 3\ln\frac{m^2}{\mu^2}\right) B^{[1]}_{Wb,born} \\ B^{[2]}_{Wb,loop,ren,FD} &= B^{[2]}_{Wb,loop,bare,FD} \,. \end{aligned} \tag{80}$$

The only divergences left in the renormalized amplitudes are of infrared origin. The infrared divergent parts are given by

$$\begin{aligned} B^{[1]}_{Wb,loop}\Big|_{IR} &= -2\Delta\left(\frac{1}{2}\Delta+\frac{1}{2}\gamma-\frac{1}{2}\ln 4\pi+\frac{5}{4}-\ln\frac{m^2-s_{67}}{\mu^2}+\frac{1}{2}\ln\frac{m^2}{\mu^2}\right)B_{Wb,born} \\ B^{[2]}_{Wb,loop}\Big|_{IR} &= -2\Delta\left(\Delta+\gamma-\ln 4\pi+\frac{3}{2}-\ln\frac{-s_{67}}{\mu^2}\right)B_{Wb,born}\,. \end{aligned} \tag{81}$$

We now turn our attention to Ward identities and finite renormalizations. In the 't Hooft-Veltman scheme γ_5 anti-commutes with the first four Dirac matrices and commutes with the remaining ones. This treatment violates a Ward identity, which has to be restored by a finite renormalization. Explicitly, one splits the left-handed interaction into a vector (γ_μ) and axial-vector [$\Gamma_{\mu 5} = 1/2(\gamma_\mu\gamma_5 - \gamma_5\gamma_\mu)$] part.

$$\gamma_\mu\frac{1}{2}(1-\gamma_5) = \frac{1}{2}\gamma_\mu - \frac{1}{4}(\gamma_\mu\gamma_5-\gamma_5\gamma_\mu)\,. \tag{82}$$

The Ward identity is restored by a finite renormalization of the axial-vector coupling:

$$\begin{aligned} \Gamma^{bare}_{\mu 5} &= Z_{axial,HV,fin}\Gamma^{renorm}_{\mu 5} \\ Z_{axial,HV,fin} &= 1+4\frac{g^2}{(4\pi)^2}C_F\,. \end{aligned} \tag{83}$$

There is some freedom in how we continue the left-handed coupling in the 't Hooft-Veltman scheme to D dimensions. For example, the expressions

$$\gamma_\mu\frac{1}{2}(1-\gamma_5)\,,\quad \frac{1}{2}(1+\gamma_5)\gamma_\mu,\quad \frac{1}{2}(1+\gamma_5)\gamma_\mu\frac{1}{2}(1-\gamma_5)\,,\quad \frac{1}{2}\gamma_\mu-\frac{1}{4}(\gamma_\mu\gamma_5-\gamma_5\gamma_\mu)\,, \tag{84}$$

all agree in four dimensions, but differ in D dimensions. Of course this difference is compensated by the appropriate finite renormalization. $Z_{axial,HV,fin}$ corresponds to the choice $-1/4(\gamma_\mu\gamma_5 - \gamma_5\gamma_\mu)$.

The four-dimensional scheme violates a Ward identity as well, which is restored by a finite renormalization of the left-handed coupling $\Gamma_{left} = 1/2\gamma_\mu(1-\gamma_5)$,

$$\begin{aligned} \Gamma^{bare}_{left} &= Z_{EW,FDfin}\Gamma^{renorm}_{left} \\ Z_{EW,FD,fin} &= 1+\frac{g^2}{(4\pi)^2}C_F\,. \end{aligned} \tag{85}$$

After the finite renormalization the renormalized amplitudes

$$\begin{aligned} A_{Wb,loop,ren,HV} &= \left(Z^{1/2}_{\psi,HV}\right)^4 A_{Wb,loop,HV} \\ A_{Wb,loop,ren,FD} &= \left(Z^{1/2}_{\psi,FD}\right)^4 (Z_{EW,FD,fin})^{-2}\, A_{Wb,loop,FD}\,, \end{aligned} \tag{86}$$

agree up to terms resulting from a different treatment of the infrared divergences. The axial-vector coupling in the 't Hooft-Veltman scheme has been renormalized according to

$$\Gamma^{bare}_{\mu 5} \quad = \quad Z_{axial,HV,fin} \Gamma^{renorm}_{\mu 5} \, . \tag{87}$$

In detail, we have for the finite parts of UV-origin in terms of $g^2/(4\pi)^2 C_F B^{Born}$

	FD	HV_{vector}	HV_{axial}
$B_{Wb,loop,bare}$	0	-2	$+2$
$Z^{-1}_{coupling}$	-1	0	-4
Z_ψ	0	$+1$	$+1$
Sum	-1	-1	-1

(88)

The remaining differences are due to finite terms of infrared origin. Due to the universal structure of the infrared divergences we may relate the amplitudes calculated in the four-dimensional scheme to the ones in the 't Hooft-Veltman scheme [73, 88, 89]. The relations are

$$\begin{aligned} B^{[1]}_{Wb,loop,HV} &= B^{[1]}_{Wb,loop,FD} - \frac{1}{2} B^{[1]}_{Wb,Born} \\ B^{[2]}_{Wb,loop,HV} &= B^{[2]}_{Wb,loop,FD} - B^{[1]}_{Wb,Born} \, . \end{aligned} \tag{89}$$

This completes our discussion on scheme-independence. In summary, we are able to perform the calculation in a four-dimensional scheme and to obtain from this result the amplitudes in the 't Hooft-Veltman scheme through simple and universal relations.

We would like to comment on the original formulation of dimensional reduction. Dimensional reduction [90,91] differs from the four-dimensional scheme by use of the relation

$$\not{p}_{(4)} \not{p}_{(4)} \quad = \quad p^2_{(D)} \cdot 1_{(4)} \, , \tag{90}$$

which can be interpreted as "D is smaller than 4". The results in dimensional reduction can easily obtained from ours by dropping the terms $C_0^{(-2\varepsilon)}$. The $C_0^{(-2\varepsilon)}$-terms yield finite terms related to UV-divergences. We note that the results in dimensional reduction cannot be related to ours, nor to the 't Hooft-Veltman scheme by a finite renormalization, since the term with $C_0^{(-2\varepsilon)}$ in $B^{[1]}_{Wb,loop}$ is not proportional to $B_{Wb,born}$. Therefore the naive approach of dimensional reduction is not consistent. The situation may be cured at the expense of introducing additional scalar ghost particles [92], however this spoils the calculational simplicity of the scheme. From a calculational point of view we prefer the scheme defined in Ref. [87], since $6 - 2\varepsilon$-dimensional integrals are rather "inexpensive" to evaluate.

4.3 Spin observables

The helicity amplitudes contain the complete spin information for the single-top-quark processes. In the old-fashioned method, spin observables are calculated by inserting the spin projection operator

$$u(p,s)\bar{u}(p,s) \quad = \quad (\not{p} + m) \frac{1}{2} (1 + \gamma_5 \not{s}) \, , \tag{91}$$

into the matrix element squared. In Eq. (91) s denotes a spin four-vector with $s^2 = -1$, and $p \cdot s = 0$. In the rest frame of the particle the spatial components of s point in the same direction as the spin of the particle [93]. To make contact with this formulation, we first introduce the spin density matrix [94] in the basis of Eq. (53):

$$\rho = \begin{pmatrix} A(...,p^+,...)A^*(...,p^+,...) & A(...,p^+,...)A^*(...,p^-,...) \\ A(...,p^-,...)A^*(...,p^+,...) & A(...,p^-,...)A^*(...,p^-,...) \end{pmatrix} . \tag{92}$$

In addition we need the projection operator Eq. (91) in the basis of Eq. (53). This one is obtained as

$$P = \frac{1}{2}\frac{1}{2pq} \begin{pmatrix} -\langle q - |(\not{p}+m)(1-\not{s})|q-\rangle & \langle q - |(\not{p}+m)(1-\not{s})|q+\rangle \\ -\langle q + |(\not{p}+m)(1-\not{s})|q-\rangle & \langle q + |(\not{p}+m)(1-\not{s})|q+\rangle \end{pmatrix} . \tag{93}$$

Spin observables are then calculated as

$$\text{Tr } (P \cdot \rho) . \tag{94}$$

Note that the entries of the matrices are complex numbers, and that the spin vector s enters only through the matrix P. It is easily verified that this expression agrees with the one obtained from Eq. (91). The spin summed result is recovered by replacing P in Eq. (94) with the unit matrix.

5 Numerical results

The inclusive NLO cross sections for s- and t-channel production of single-top-quarks were published in Refs. [56] and [58], respectively. After we choose our numerical inputs, we compare to these older calculations, and update the inclusive cross sections using newer parton distribution functions (PDFs).

In order to make a definite comparison to the older calculations, we reevaluate all results with the following parameters: For the mass of the W boson we use $m_W = 80.4$ GeV. For the top-quark mass we take $m_t = 175$ GeV. In LO calculations we use CTEQ5L PDFs [42]. In NLO calculations we use CTEQ5M1 PDFs with 2-loop running of α_s. We define the electroweak coupling by $g^2 = 8G_F M_W^2/\sqrt{2}$, with Fermi coupling constant of $G_F = 1.16639 \times 10^{-5}$ GeV^{-2}. We consider $p\bar{p}$ collisions with center-of-momentum energy $\sqrt{S} = 1.8$, 1.96, or 2.0 TeV (Tevatron), and pp collisions with a center-of-momentum energy $\sqrt{S} = 14$ TeV (LHC).

Unlike the massive dipole formalism, the phase space slicing method of two cutoffs depends on explicit parameters δ_s and δ_c. In Figs. 3 and 4 we show the s- and t-channel inclusive cross sections as a function of $\delta_s = 300 \times \delta_c$. The logarithmic dependence cancels in the sum of the two- and three-body contributions and leaves terms proportional to δ_s and δ_c. By taking $\delta_s <$ a few $\times 10^{-3}$, the cross sections converge to the updated analytic results.

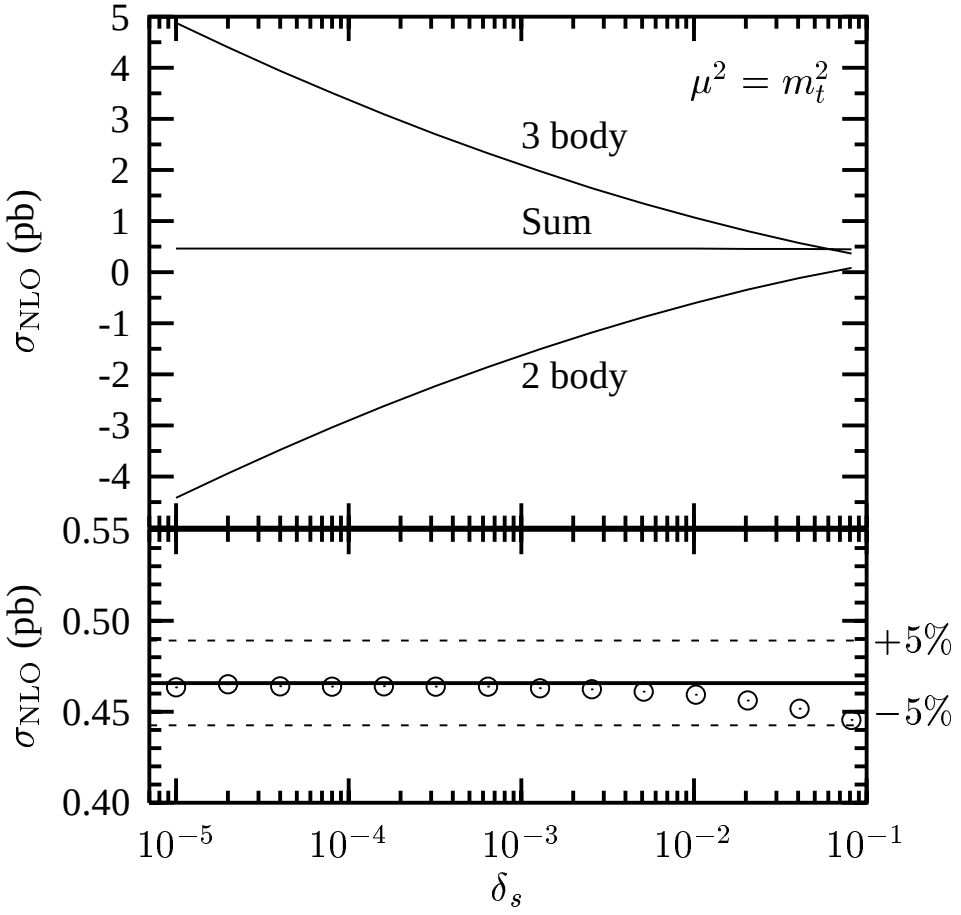

Figure 3: The next-to-leading order single-top-quark total cross section for the s-channel at a $\sqrt{S} = 2$ TeV proton-antiproton machine. The two- and three- body contributions, together with their sum, are shown as a function of the soft cutoff δ_s. The bottom enlargement shows the sum (open circles) relative to ±5% (dotted lines) of the analytic result (solid line).

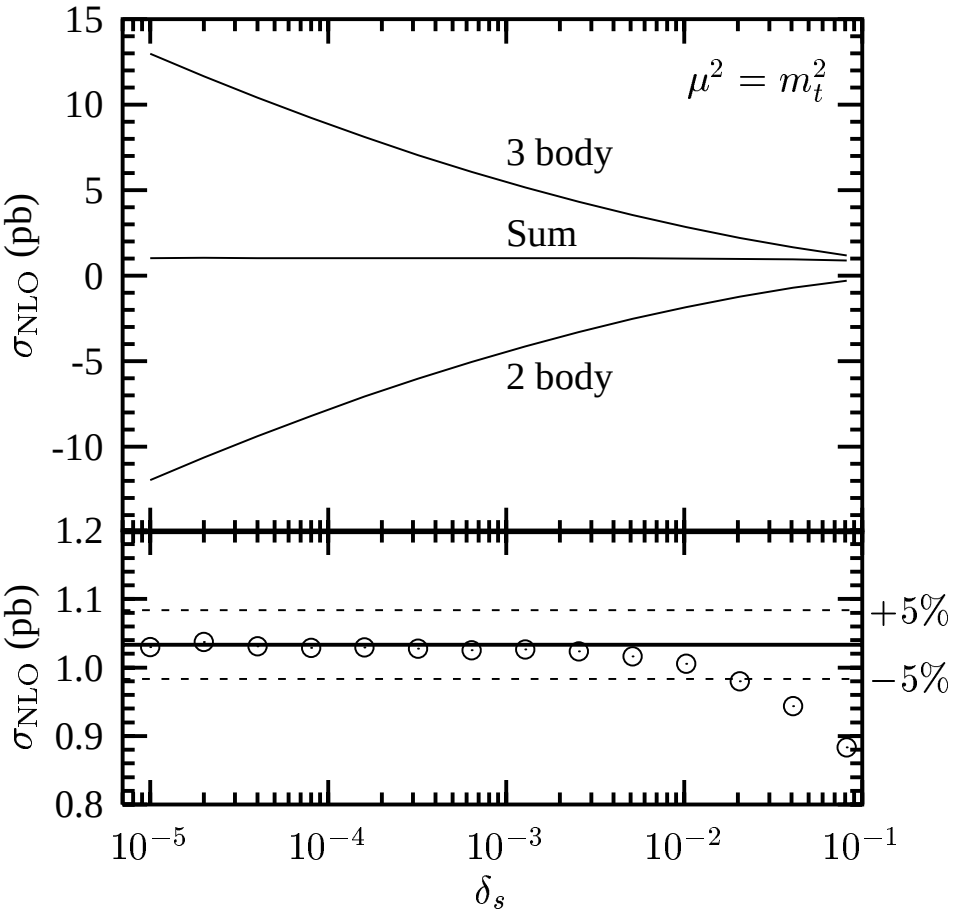

Figure 4: The next-to-leading order single-top-quark total cross section for the t-channel at a $\sqrt{S} = 2$ TeV proton-antiproton machine. The two- and three- body contributions, together with their sum, are shown as a function of the soft cutoff δ_s. The bottom enlargement shows the sum (open circles) relative to $\pm 5\%$ (dotted lines) of the analytic result (solid line).

Table 1: LO and NLO cross sections for single-top-quark production at the Tevatron and LHC for $m_t = 175$ GeV. Cross sections are evaluated with CTEQ5L and CTEQ5M1 PDFs, and all scales set to m_t. Errors include only Monte Carlo statistics.

Process	$\sqrt{S}$	σ_{LO} (pb)	σ_{NLO} (pb)
s-channel	1.8 TeV $p\bar{p}$ (t)	0.259	0.380 $\pm$0.002
	1.96 TeV $p\bar{p}$ (t)	0.304	0.447 $\pm$0.002
	2 TeV $p\bar{p}$ (t)	0.315	0.463 $\pm$0.002
	14 TeV pp (t)	4.53	6.55 $\pm$0.03
	14 TeV pp $(\bar{t})$	2.74	4.07 $\pm$0.02
t-channel	1.8 TeV $p\bar{p}$ (t)	0.648	0.702 $\pm$0.003
	1.96 TeV $p\bar{p}$ (t)	0.883	0.959 $\pm$0.002
	2 TeV $p\bar{p}$ (t)	0.948	1.029 $\pm$0.004
	14 TeV pp (t)	144.8	152.6 $\pm$0.6
	14 TeV pp $(\bar{t})$	83.4	90.0 $\pm$0.5

The LO and NLO cross sections for s-channel and t-channel single-top-quark production are listed in picobarns in Tables 1 and 2. Since the Tevatron is a $p\bar{p}$ collider, the cross sections for top-quark (t) and antitop-quark ($\bar{t}$) production are the same. The LHC is a pp collider, and hence the t and $\bar{t}$ cross sections are listed separately. Factorization (μ_F) and renormalization (μ_R) scales are set equal. In Table 1 all scales are set to the top mass m_t. In Table 2 the s-channel cross sections are calculated using the invariant mass of the top-quark/antibottom-jet pair for the scale, $\mu^2 = M^2_{t\bar{b}} = (P_t + P_{\bar{b}})^2$, where P_t and $P_{\bar{b}}$ are the four-momenta of the top quark and antibottom jet, respectively.[1] The t-channel cross section uses the double deep-inelastic-scattering (DDIS) scales, $\mu_l^2 = Q^2 = -(p_b - p_t)^2$ for the light-quark line and $\mu_h^2 = Q^2 + m_t^2 = -(p_u - p_d)^2 + m_t^2$ for the heavy-quark line, where Q^2 is the virtuality of the exchanged W boson (valid through NLO), and p_i are the four-momenta of the partons in Eq. (1). All LO cross sections are identical to those in Refs. [56] and [58] once updated to the CTEQ5 PDFs.

We compare the NLO s-channel cross sections to a recoding of Refs. [95] and [56]. The results agree to within 1% for all scale choices. Of note is our use of $M_{t\bar{b}}$ for the scale in Table 2 rather than Q^2, the virtuality of the W, which was used in Ref. [56]. These two scales are identical at LO and in initial-state corrections, but differ by the emitted gluon in final state corrections. Since we are interested in making cuts based on observables, such as $M_{t\bar{b}}$, we choose this as the scale. While the central value of any of the scale choices is very similar, the uncertainty is slightly larger at NLO using m_t or $M_{t\bar{b}}$. In particular, if we vary the scales between $M_{t\bar{b}}/2$ and $2M_{t\bar{b}}$ (or $m_t/2$ and $2m_t$), we find the s-channel cross section varies by $+7.8 - 6.9\%$ at LO, and $+5.7 - 5.0\%$ ($+5.5 - 4.6\%$) at NLO. In contrast,

[1] The choice of jet definition induces a cone-size dependence in the scale that always enters the cross section at one higher order in QCD. We have confirmed that this effect is numerically less than the overall scale uncertainty for any infrared-safe jet definition.

Table 2: LO and NLO cross sections for single-top-quark production at the Tevatron and LHC for $m_t = 175$ GeV. Cross sections are evaluated with CTEQ5L and CTEQ5M1 PDFs, and $M_{t\bar{b}}$ or the DDIS scales ($\mu_l = Q^2$, $\mu_h = Q^2 + m_t^2$), for s-channel or t-channel, respectively. Errors include only Monte Carlo statistics.

Process	$\sqrt{S}$	σ_{LO} (pb)	σ_{NLO} (pb)
s-channel	1.8 TeV $p\bar{p}$ (t)	0.244	0.377 $\pm$0.002
	1.96 TeV $p\bar{p}$ (t)	0.287	0.442 $\pm$0.002
	2 TeV $p\bar{p}$ (t)	0.297	0.459 $\pm$0.002
	14 TeV pp (t)	4.612	6.56 $\pm$0.03
	14 TeV pp $(\bar{t})$	2.788	4.09 $\pm$0.02
t-channel	1.8 TeV $p\bar{p}$ (t)	0.735	0.725 $\pm$0.003
	1.96 TeV $p\bar{p}$ (t)	0.996	0.990 $\pm$0.002
	2 TeV $p\bar{p}$ (t)	1.068	1.062 $\pm$0.004
	14 TeV pp (t)	152.7	155.9 $\pm$0.6
	14 TeV pp $(\bar{t})$	86.1	90.7 $\pm$0.5

using a scale of Q^2, as in Ref. [56], would predict a NLO scale uncertainty of $\pm 4\%$. Given that we can probe a more restricted phase space with cuts, we take the conservative view that $\pm 5.7\%$ is an appropriate estimate of the NLO scale uncertainty at the Tevatron when looking at exclusive final states. At the LHC the scale uncertainty is less than $\pm 2\%$.

At LO and NLO, but not NNLO, color conservation forbids the exchange of a gluon between the light- and heavy-quark lines. Hence, the t-channel process may be factorized at NLO into two independent corrections that each resemble deep-inelastic-scattering. The NLO t-channel cross sections in Ref. [58] were calculated using the scales suggested by this relation to double deep-inelastic-scattering. When using the DDIS scales, our results in Table 2 match the updated Ref. [58] to better than 0.3% at the Tevatron, but are larger by 2.9% at the LHC. The cross sections in Table 1 agree with the updated results of Ref. [58] to within 1% when evaluated at $\mu = m_t$. In all cases, the dipole subtraction calculations and phase space slicing calculations agree within the statistical errors.

A subtle issue arises in attempting to ascertain the effect of higher orders by varying the scale. In Ref. [58] only the scales in the vertex and PDFs of the heavy-quark line ($b \to t$) were varied because the corrections to the light-quark structure function are small.[2] However, to the extent this process looks like double deep-inelastic-scattering, we expect a similarly small effect for the heavy-quark corrections as well. Indeed, the results for LO and NLO are nearly identical when using the DDIS scales, but differ significantly when using a fixed scale such as m_t. In Table 3 we show the effects of varying the scales at the Tevatron ($\sqrt{S} = 2$ TeV) together, and separately in the light- and heavy-quark lines. What we see is that varying the scales together at LO, particularly when using m_t, severely

[2]The NLO correction to the light-quark line effectively undoes the extraction of the NLO PDFs from the DIS data.

Table 3: Scale variation of the LO and NLO cross sections for t-channel single-top-quark production at the Tevatron ($\sqrt{S} = 2$ TeV). Variation in the light-quark and heavy-quark lines are listed as μ_l and μ_h, respectively. Fixed ($\mu = m_t$), and double deep-inelastic-scattering scales are shown separately.

	σ_t	μ_h & μ_l	μ_h	μ_l
LO$_t$ (m_t)	0.95 pb	$\pm 1\%$	$^{-7.5}_{+5.5}\%$	$^{+6.7}_{-5.8}\%$
NLO$_t$ (m_t)	1.03 pb	$\pm 2.5\%$	$^{-3.5}_{+4.0}\%$	$\pm 1\%$
LO$_t$ (DDIS)	1.07 pb	$^{+0.1}_{-2}\%$	$^{-7.2}_{+5.2}\%$	$^{+8}_{-6.8}\%$
NLO$_t$ (DDIS)	1.06 pb	$\pm 3.5\%$	$^{-3}_{+4}\%$	$\pm 0.6\%$

underestimates the NLO correction.

The reason for the underestimate in varying the scales together is a series of accidental cancellations that are driven by the range of proton momentum fraction probed at the Tevatron. For a top mass of 175 GeV and a machine of around 2 TeV, the typical $x \sim 0.1$. For scales also around 100–200 GeV, the b PDF happens to increase with increasing scale, whereas the valence quarks decrease. This may be seen in the opposite signs in the last two columns of Table 3. The net effect is that to estimate the uncertainty, we must vary the scales independently, and then add them in quadrature.[3] This leads to a LO uncertainty of $\sim \pm 10\%$, and a NLO uncertainty for the Tevatron of $\pm 4\%$. At the LHC, the NLO uncertainty is $\pm 3\%$. These uncertainties are consistent with expected higher-order corrections, and with both fixed and DDIS scale choices.

While the s-channel cross section has only changed by a couple of percent from [56], the t-channel cross section is 13% smaller at the Tevatron than appears in [58]. The shift in the NLO t-channel cross section is due to the correction of bugs that appeared in the evolution of the gluon PDF in all of the older MRS and CTEQ NLO PDFs [96]. Because the b PDF is constructed almost entirely out of gluon evolution [58, 97], the effect of the bug is greatly enhanced in all processes where there is a c or b quark in the initial state. The programming bug is corrected in MRS99 (updated) [43] and CTEQ5M1 [42].

The central goal of our calculations is not to recalculate inclusive cross sections, but to provide full momentum and spin dependent distributions with the option for arbitrary cuts. Detailed analyses of the phenomenological issues concerning these distributions will be presented elsewhere [98]. Here we restrict ourselves to a comparison of the results using the phase space slicing method and massive dipole formalism.

For our comparisons we reconstruct jets using a k_T cluster algorithm [99] with $\Delta R = 1$. We define a simple detector acceptance by assuming that only jets with $p_T > 20$ GeV and $|\eta| < 2$ are observed. We calculate all cross sections at the scale $\mu = m_t = 175$ GeV, and at a 2 TeV $p\bar{p}$ collider.

[3]The light- and heavy-quark corrections are factorizable through NLO, and hence are only weakly correlated through the evolution of the PDFs.

In Figs. 5 and 6 we present the NLO transverse momentum p_{Tb} and pseudorapidity η_b distributions of the b-jet in s-channel production of a top quark, with cuts based on the "jet veto" search strategy in Ref. [8]. We accept events where only the top-quark and b-jet pass the cuts above, and any additional jets are either soft ($p_{Tj} < 20$ GeV) or are outside the simple detector ($|\eta_j| > 2$). The phase space slicing method and massive dipole formalism give identical distributions, even in this region of restricted phase space.

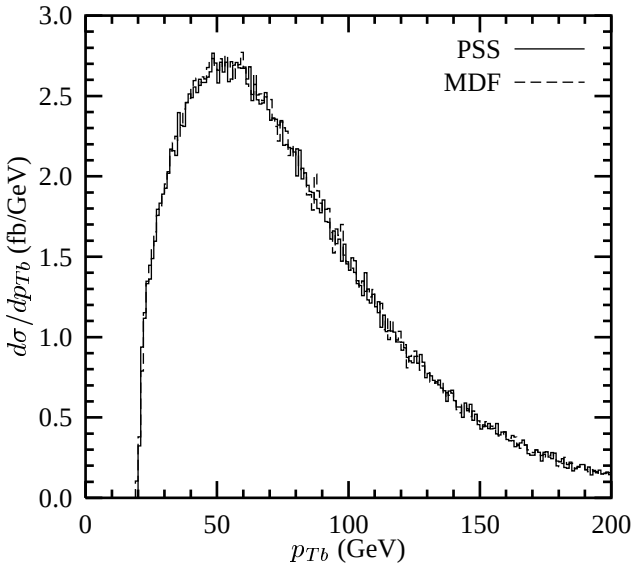

Figure 5: Transverse momentum distribution of the b-jet at NLO in s-channel production of a top quark at the Tevatron ($\sqrt{S} = 2$ TeV) after cuts. Phase space slicing (PSS) results (solid) and massive dipole formalism (MDF) results (dashed) are both shown.

In Figs. 7 and 8 we present the NLO transverse momentum p_{Tj_1} and pseudorapidity η_{j_1} distributions of the highest-p_T jet in t-channel production of a top quark, using the same "jet veto" search strategy as above. We accept events where only the top-quark and highest-p_T jet pass the cuts above, and any additional jets are either soft ($p_{Tj_2} < 20$ GeV) or are outside the simple detector ($|\eta_{j_2}| > 2$). The phase space slicing method and massive dipole formalism predict identical distributions at NLO.

6 Conclusions

We present three independent calculations of the fully differential production of a single top quark plus one jet at next-to-leading order in hadronic collisions. At this order in QCD the cross sections factorize into two non-interfering production modes that may be identified by the s-channel or t-channel exchange of a W boson. The s-channel cross section is characterized by having a typical final state of a top quark and a bottom-quark jet. The jet in the t-channel cross section tends to be somewhat more forward, and rarely contains a bottom quark. New physics scenarios tend to effect these production modes

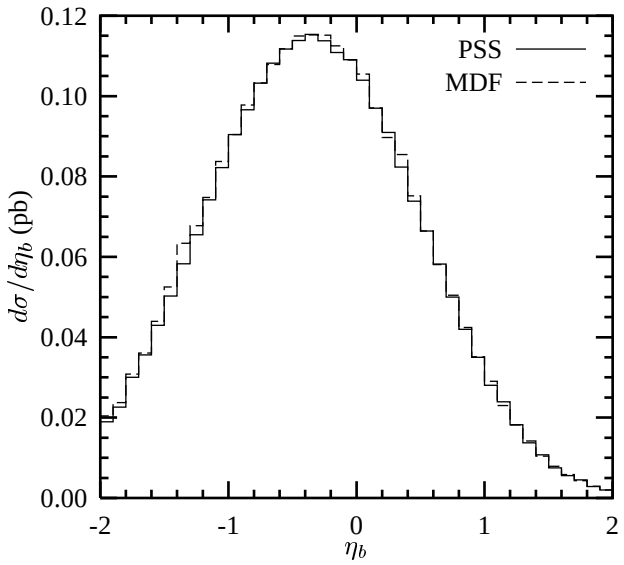

Figure 6: Pseudorapidity distribution of the b-jet at NLO in s-channel production of a top quark at the Tevatron ($\sqrt{S} = 2$ TeV) after cuts. Phase space slicing (PSS) results (solid) and massive dipole formalism (MDF) results (dashed) are both shown.

differently, and hence an accurate measurement and theoretical calculation of both modes is desirable. Further, the CKM matrix element $|V_{tb}|^2$ is directly proportional to the cross section, and the ability to extract V_{tb} is ultimately limited by our ability to predict the measured exclusive cross sections with experimental cuts.

The total cross sections for s- and t-channel production are updated with CTEQ5 parton distribution functions for runs I and II of the Tevatron, and for the LHC. The t-channel cross section is smaller than previously published by 13%. This decrease is due entirely to the correction of a bug in the parton distribution functions. If the Tevatron continues to run at 1.96 TeV instead of 2 TeV, the $s(t)$-channel production modes will produce 4%(7%) fewer events than previously expected. We discuss some subtleties in estimating the effects of higher-order corrections on these cross sections.

We show that the phase space slicing methods of one and two cutoffs and the massive dipole formalism produce the same jet distributions and cross sections. The dipole calculation retains the full spin dependence of the external particles, and so may be used to predict spin-dependent correlations of the partons. We discuss elsewhere [98] the effects of top-quark mass, scales, jet definitions, and parton distribution functions on the shapes of the NLO distributions.

Acknowledgments

B.H. and Z.S. thank Argonne National Laboratory High Energy Physics Division for support during the early stages of the project. Their work was supported in part by the U.S. Department of Energy, High Energy Physics Division, under contract W-31-109-Eng-38,

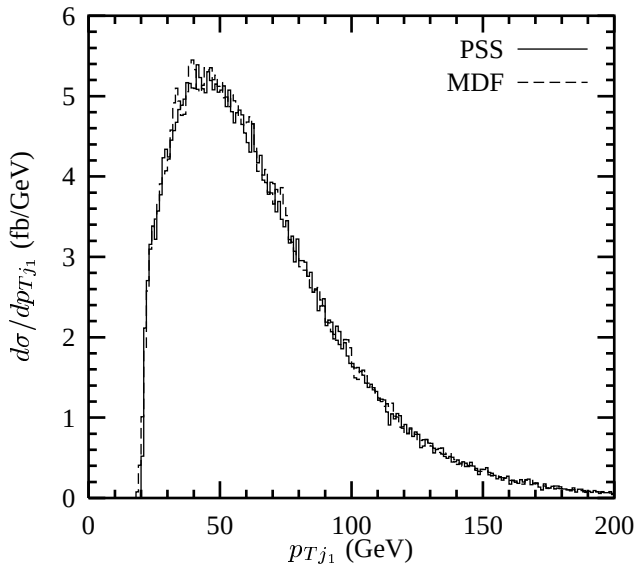

Figure 7: Transverse momentum distribution of the highest-p_T jet (j_1) at NLO in t-channel production of a top quark at the Tevatron ($\sqrt{S} = 2$ TeV) after cuts. Phase space slicing (PSS) results (solid) and massive dipole formalism (MDF) results (dashed) are both shown.

and DE-AC02-76CH03000 (at Fermilab). The work of E.L. and L.P. is supported by the Foundation for Fundamental Research of Matter (FOM) and the National Organization for Scientific Research (NWO).

A Scalar integrals

We calculate the integrals in $D = 4 - 2\varepsilon$ dimensions and use the notation

$$\Delta \;=\; \frac{1}{\varepsilon} - \gamma + \ln 4\pi \,. \tag{95}$$

All integrals are calculated in the Euclidean region (invariants $p^2 < 0$ and masses $m^2 > 0$). These expressions can then be continued analytically to the regions of interest, using the substitution $-s \to -s - i\varepsilon$ (where ε denotes a small parameter, not to be confused with the one appearing in dimensional regularization) and the formula

$$\ln(-s - i\varepsilon) \;=\; \ln(|s|) - i\pi\Theta(s) \,. \tag{96}$$

Massive integrals: The tadpole is given for $m^2 > 0$ by

$$\begin{aligned} A_0(m^2) &= (4\pi)^2\mu^{4-D} \int \frac{d^Dk}{(2\pi)^D i} \frac{1}{k^2 - m^2} = -m^2\Gamma(-1+\varepsilon)(4\pi)^\varepsilon \left(\frac{m^2}{\mu^2}\right)^{-\varepsilon} \\ &= m^2 \left(\Delta + 1 - \ln\frac{m^2}{\mu^2}\right) + O(\varepsilon) \,. \end{aligned} \tag{97}$$

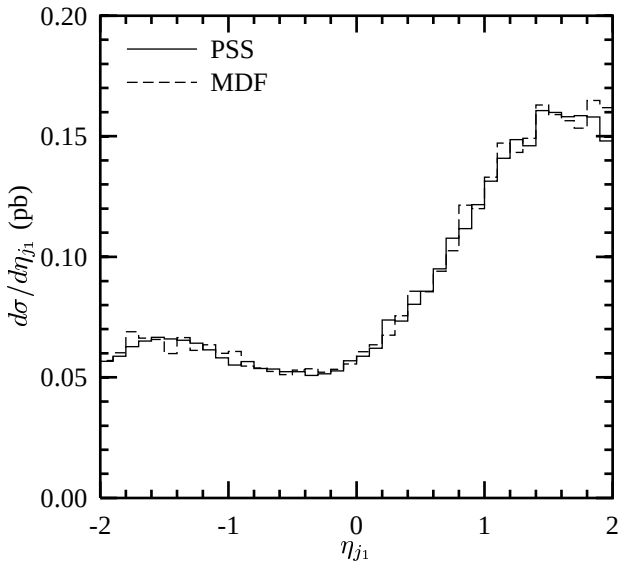

Figure 8: Pseudorapidity distribution of the highest-p_T jet (j_1) at NLO in t-channel production of a top quark at the Tevatron ($\sqrt{S} = 2$ TeV) after cuts. Phase space slicing (PSS) results (solid) and massive dipole formalism (MDF) results (dashed) are both shown.

The bubble with one internal mass is given for $-p^2 > 0, m^2 > 0$ by

$$\begin{aligned} B_0^{(a)}(p^2, m^2) &= (4\pi)^2 \mu^{4-D} \int \frac{d^D k}{(2\pi)^D i} \frac{1}{k^2((k-p)^2 - m^2)} \\ &= \Delta + 2 - \ln \frac{m^2 - p^2}{\mu^2} + \frac{m^2}{-p^2} \ln \frac{m^2}{m^2 - p^2} + O(\varepsilon)\,. \end{aligned} \tag{98}$$

On-shell integrals: The bubble with one internal mass is given for $p^2 = m^2 > 0$ by

$$\begin{aligned} B_0^{(b)}(m^2) &= (4\pi)^2 \mu^{4-D} \int \frac{d^D k}{(2\pi)^D i} \frac{1}{k^2((k-p)^2 - m^2)} \\ &= \Delta + 2 - \ln \frac{m^2}{\mu^2} + O(\varepsilon)\,. \end{aligned} \tag{99}$$

The triangle with two external masses and one internal mass, between the two external massive lines is given for $p_1^2 = 0$, $(p_1 + p_2)^2 = m^2 > 0$ by

$$\begin{aligned} C_0^{(a)}(p_2^2, m^2) &= (4\pi)^2 \mu^{4-D} \int \frac{d^D k}{(2\pi)^D i} \frac{1}{k^2 (k-p_1)^2 ((k-p_1-p_2)^2 - m^2)} \\ &= \left(4\pi\mu^2\right)^{\varepsilon} \frac{\Gamma(1+\varepsilon)}{m^2 - p_2^2} \left\{ -\frac{1}{2\varepsilon^2} + \frac{1}{\varepsilon} \left(\ln\left(m^2 - p_2^2\right) - \frac{1}{2} \ln(m^2) \right) \right. \\ &\quad \left. + \frac{1}{4} \ln^2(m^2) - \frac{1}{2} \ln^2\left(m^2 - p_2^2\right) + \mathrm{Li}_2\left(\frac{-p_2^2}{m^2 - p_2^2} \right) \right\} + O(\varepsilon) \end{aligned}$$

$$= \frac{1}{m^2-p_2^2}\left\{-\frac{1}{2}\Delta^2+\Delta\left(-\frac{1}{2}\gamma+\frac{1}{2}\ln 4\pi+\frac{1}{2}\ln\frac{m^2}{\mu^2}+\ln\frac{m^2-p_2^2}{m^2}\right)-\frac{1}{4}\left(\gamma-\ln 4\pi\right)^2\right.$$
$$\left.+\frac{1}{4}\ln^2\left(\frac{m^2}{\mu^2}\right)-\frac{1}{2}\ln^2\left(\frac{m^2-p_2^2}{\mu^2}\right)+\ \mathrm{Li}_2\left(\frac{-p_2^2}{m^2-p_2^2}\right)-\frac{\pi^2}{24}\right\}+O(\varepsilon)\,. \tag{100}$$

Integrals with no internal masses: The bubble with $-p^2>0$ is given by

$$B_0^{(c)}(p^2) = (4\pi)^2\mu^{4-D}\int\frac{d^Dk}{(2\pi)^Di}\frac{1}{k^2(k-p)^2}=\Gamma(\varepsilon)\frac{\Gamma^2(1-\varepsilon)}{\Gamma(2-2\varepsilon)}(4\pi)^\varepsilon\left(\frac{-p^2}{\mu^2}\right)^{-\varepsilon}$$
$$= \Delta+2-\ln\frac{-p^2}{\mu^2}+O(\varepsilon)\,. \tag{101}$$

The triangle with one external mass $p_1^2=p_2^2=0$, $-s=-2p_1p_2>0$ is given by

$$C_0^{(b)}(s) = (4\pi)^2\mu^{4-D}\int\frac{d^Dk}{(2\pi)^Di}\frac{1}{k^2(k-p_1)^2(k-p_1-p_2)^2}$$
$$= \frac{1}{s}\frac{1}{\varepsilon^2}\frac{\Gamma(1+\varepsilon)\Gamma^2(1-\varepsilon)}{\Gamma(1-2\varepsilon)}(4\pi)^\varepsilon\left(\frac{-s}{\mu^2}\right)^{-\varepsilon}$$
$$= \frac{1}{s}\left(\Delta^2+\Delta\left(\gamma-\ln 4\pi-\ln\frac{-s}{\mu^2}\right)+\frac{1}{2}\left(\gamma-\ln 4\pi\right)^2+\frac{1}{2}\ln^2\left(\frac{-s}{\mu^2}\right)-\frac{\pi^2}{12}\right)+O(\varepsilon)\,. \tag{102}$$

Six-dimensional integrals: The triangle with an additional power of $k^2_{-2\varepsilon}$ in the numerator is equivalent to an integral in $D=6-2\varepsilon$ dimensions and yields for the massless and massive case

$$C_0^{(-2\varepsilon)} = (4\pi)^2\mu^{4-D}\int\frac{d^Dk}{(2\pi)^Di}\frac{k^2_{(-2\varepsilon)}}{k^2(k-p_1)^2((k-p_1-p_2)^2-m^2)}$$
$$= -\frac{1}{2}+O(\varepsilon)\,. \tag{103}$$

References

[1] S. S. Willenbrock and D. A. Dicus, Phys. Rev. D **34**, 155 (1986).

[2] C. P. Yuan, Phys. Rev. D **41**, 42 (1990).

[3] S. Cortese and R. Petronzio, Phys. Lett. B **253**, 494 (1991).

[4] R. K. Ellis and S. Parke, Phys. Rev. D **46**, 3785 (1992).

[5] D. O. Carlson and C. P. Yuan, Phys. Lett. B **306**, 386 (1993).

[6] T. Stelzer and S. Willenbrock, Phys. Lett. B **357**, 125 (1995).

[7] A. P. Heinson, A. S. Belyaev and E. E. Boos, Phys. Rev. D **56**, 3114 (1997).

[8] T. Stelzer, Z. Sullivan and S. Willenbrock, Phys. Rev. D **58**, 094021 (1998).

[9] M. Beneke *et al.*, in *Proceedings of the Workshop on Standard Model Physics (and More) at the LHC*, eds. G. Altarelli, and M. L. Mangano (CERN, Geneva, 2000), p. 456, arXiv:hep-ph/0003033.

[10] V. M. Abazov *et al.* [D0 Collaboration], Phys. Lett. B **517**, 282 (2001); B. Abbott *et al.* [D0 Collaboration], Phys. Rev. D **63**, 031101 (2001); A. P. Heinson [D0 Collaboration], Int. J. Mod. Phys. A **16S1A**, 386 (2001).

[11] C. I. Ciobanu [CDF Collaboration], Int. J. Mod. Phys. A **16S1A**, 389 (2001); D. Acosta *et al.* [CDF Collaboration], Phys. Rev. D **65**, 091102 (2002); T. Kikuchi, S. K. Wolinski, L. Demortier, S. Kim, and P. Savard [CDF Collaboration], Int. J. Mod. Phys. A **16S1A**, 382 (2001).

[12] G. Mahlon and S. Parke, Phys. Rev. D **55**, 7249 (1997).

[13] G. Mahlon and S. Parke, Phys. Lett. B **476**, 323 (2000).

[14] R. D. Peccei and X. Zhang, Nucl. Phys. B **337**, 269 (1990); R. D. Peccei, S. Peris and X. Zhang, Nucl. Phys. B **349**, 305 (1991).

[15] D. O. Carlson, E. Malkawi, and C. P. Yuan, Phys. Lett. B **337**, 145 (1994).

[16] G. L. Kane, G. A. Ladinsky and C. P. Yuan, Phys. Rev. D **45**, 124 (1992).

[17] T. G. Rizzo, Phys. Rev. D **53**, 6218 (1996).

[18] T. Tait and C. P. Yuan, Phys. Rev. D **55**, 7300 (1997).

[19] A. Datta and X. Zhang, Phys. Rev. D **55**, 2530 (1997).

[20] K. Whisnant, J. M. Yang, B. L. Young and X. Zhang, Phys. Rev. D **56**, 467 (1997).

[21] E. Boos, L. Dudko and T. Ohl, Eur. Phys. J. C **11**, 473 (1999).

[22] T. Tait and C. P. Yuan, Phys. Rev. D **63**, 014018 (2001).

[23] D. Espriu and J. Manzano, Phys. Rev. D **65**, 073005 (2002).

[24] E. H. Simmons, Phys. Rev. D **55**, 5494 (1997).

[25] G. Lu, Y. Cao, J. Huang, J. Zhang and Z. Xiao, arXiv:hep-ph/9701406.

[26] P. Baringer, P. Jain, D. W. McKay and L. L. Smith, Phys. Rev. D **56**, 2914 (1997).

[27] C. X. Yue and G. R. Lu, Chin. Phys. Lett. **15**, 631 (1998).

[28] T. Tait and C. P. Yuan, arXiv:hep-ph/9710372.

[29] T. Han, M. Hosch, K. Whisnant, B. L. Young and X. Zhang, Phys. Rev. D **58**, 073008 (1998).

[30] D. Atwood, S. Bar-Shalom, G. Eilam and A. Soni, Phys. Rev. D **54**, 5412 (1996).

[31] S. Bar-Shalom, D. Atwood and A. Soni, Phys. Rev. D **57**, 1495 (1998).

[32] E. Christova, S. Fichtinger, S. Kraml and W. Majerotto, Phys. Rev. D **65**, 094002 (2002).

[33] C. S. Li, R. J. Oakes and J. M. Yang, Phys. Rev. D **55**, 1672 (1997).

[34] C. S. Li, R. J. Oakes and J. M. Yang, Phys. Rev. D **55**, 5780 (1997).

[35] C. S. Li, R. J. Oakes, J. M. Yang and H. Y. Zhou, Phys. Rev. D **57**, 2009 (1998).

[36] A. Datta, J. M. Yang, B. L. Young and X. Zhang, Phys. Rev. D **56**, 3107 (1997).

[37] R. J. Oakes, K. Whisnant, J. M. Yang, B. L. Young and X. Zhang, Phys. Rev. D **57**, 534 (1998).

[38] K. i. Hikasa, J. M. Yang and B. L. Young, Phys. Rev. D **60**, 114041 (1999).

[39] P. Chiappetta, A. Deandrea, E. Nagy, S. Negroni, G. Polesello and J. M. Virey, Phys. Rev. D **61**, 115008 (2000).

[40] A. Datta, P. J. O'Donnell, Z. H. Lin, X. Zhang and T. Huang, Phys. Lett. B **483**, 203 (2000).

[41] H. L. Lai *et al.* [CTEQ Collaboration], Phys. Rev. D **55**, 1280 (1997).

[42] H. L. Lai *et al.* [CTEQ Collaboration], Eur. Phys. J. C **12**, 375 (2000).

[43] A. D. Martin, R. G. Roberts, W. J. Stirling and R. S. Thorne, Eur. Phys. J. C **14**, 133 (2000).

[44] J. C. Collins and W.-K. Tung, Nucl. Phys. B **278**, 934 (1986).

[45] M. A. Aivazis, J. C. Collins, F. I. Olness and W. K. Tung, Phys. Rev. D **50**, 3102 (1994).

[46] M. Buza, Y. Matiounine, J. Smith and W. L. van Neerven, Eur. Phys. J. C **1**, 301 (1998).

[47] J. Smith, arXiv:hep-ph/9708212.

[48] A. Chuvakin, J. Smith and W. L. van Neerven, Phys. Rev. D **61**, 096004 (2000).

[49] R. S. Thorne and R. G. Roberts, Phys. Lett. B **421**, 303 (1998).

[50] R. S. Thorne and R. G. Roberts, Phys. Rev. D **57**, 6871 (1998).

[51] M. Carena *et al.*, arXiv:hep-ph/0010338.

[52] S. Abel *et al.* [SUGRA Working Group Collaboration], arXiv:hep-ph/0003154.

[53] E. L. Berger, B. W. Harris and Z. Sullivan, Phys. Rev. Lett. **83**, 4472 (1999).

[54] B. Allanach *et al.*, arXiv:hep-ph/9906224.

[55] G. Bordes and B. van Eijk, Nucl. Phys. B **435**, 23 (1995).

[56] M. C. Smith and S. Willenbrock, Phys. Rev. D **54**, 6696 (1996).

[57] S. Mrenna and C. P. Yuan, Phys. Lett. B **416**, 200 (1998).

[58] T. Stelzer, Z. Sullivan, and S. Willenbrock, Phys. Rev. D **56**, 5919 (1997).

[59] K. Fabricius, I. Schmitt, G. Kramer and G. Schierholz, Z. Phys. C **11**, 315 (1981).

[60] G. Kramer and B. Lampe, Fortsch. Phys. **37**, 161 (1989).

[61] L. J. Bergmann, *Next-to-leading-log QCD calculation of symmetric dihadron production*, Ph.D. thesis, Florida State University, 1989.

[62] H. Baer, J. Ohnemus, and J. F. Owens, Phys. Rev. D **40**, 2844 (1989).

[63] W. T. Giele and E. W. N. Glover, Phys. Rev. D **46**, 1980 (1992).

[64] W. T. Giele, E. W. N. Glover, and D. A. Kosower, Nucl. Phys. B **403**, 633 (1993).

[65] S. Keller and E. Laenen, Phys. Rev. D **59**, 114004 (1999).

[66] B. W. Harris and J. F. Owens, Phys. Rev. D **65**, 094032 (2002).

[67] R. K. Ellis, D. A. Ross and A. E. Terrano, Nucl. Phys. B **178**, 421 (1981).

[68] Z. Kunszt and P. Nason, in *Z Physics LEP 1*, Proceedings of the Workshop, Geneva, Switzerland, 1989, ed. by G. Altarelli, R. Kleiss and C. Verzegnassi (CERN, Geneva, 1989), Vol. 1, p. 373.

[69] Z. Kunszt and D. E. Soper, Phys. Rev. D **46**, 192 (1992).

[70] M. L. Mangano, P. Nason and G. Ridolfi, Nucl. Phys. B **373**, 295 (1992).

[71] S. Frixione, Z. Kunszt, and A. Signer, Nucl. Phys. B **467**, 399 (1996).

[72] S. Catani and M. H. Seymour, Nucl. Phys. B **485**, 291 (1997).

[73] L. Phaf and S. Weinzierl, JHEP **0104**, 006 (2001).

[74] S. Catani, S. Dittmaier, M. H. Seymour and Z. Trocsanyi, Nucl. Phys. B **627**, 189 (2002).

[75] A. S. Belyaev, E. E. Boos, and L. V. Dudko, Phys. Rev. D **59**, 075001 (1999).

[76] T. M. P. Tait, Phys. Rev. D **61**, 034001 (2000).

[77] A. Belyaev and E. Boos, Phys. Rev. D **63**, 034012 (2001).

[78] T. Gottschalk, Phys. Rev. D **23**, 56 (1981).

[79] M. Gluck, S. Kretzer and E. Reya, Phys. Lett. B **380**, 171 (1996) [Erratum-ibid. B **405**, 391 (1997)].

[80] M. L. Mangano and S. J. Parke, Phys. Rept. **200**, 301 (1991).

[81] L. J. Dixon, arXiv:hep-ph/9601359.

[82] R. Kleiss and W. J. Stirling, Nucl. Phys. B **262**, 235 (1985).

[83] F. A. Berends, P. H. Daverveldt, and R. Kleiss, Nucl. Phys. B **253**, 441 (1985).

[84] A. Ballestrero and E. Maina, Phys. Lett. B **350**, 225 (1995).

[85] S. Dittmaier, Phys. Rev. D **59**, 016007 (1999).

[86] J. van der Heide, E. Laenen, L. Phaf, and S. Weinzierl, Phys. Rev. D **62**, 074025 (2000).

[87] S. Weinzierl, arXiv:hep-ph/9903380.

[88] Z. Kunszt, A. Signer, and Z. Trocsanyi, Nucl. Phys. B **411**, 397 (1994).

[89] S. Catani, M. H. Seymour, and Z. Trocsanyi, Phys. Rev. D **55**, 6819 (1997).

[90] W. Siegel, Phys. Lett. B **84**, 193 (1979).

[91] W. Siegel, Phys. Lett. B **94**, 37 (1980).

[92] D. M. Capper, D. R. T. Jones, and P. van Nieuwenhuizen, Nucl. Phys. B **167**, 479 (1980).

[93] G. Mahlon and S. Parke, Phys. Rev. D **53**, 4886 (1996).

[94] A. Brandenburg, M. Flesch, and P. Uwer, Phys. Rev. D **59**, 014001 (1999).

[95] T. H. Chang, K. J. Gaemers and W. L. van Neerven, Nucl. Phys. B **202**, 407 (1982).

[96] J. Blumlein, *et al.*, in *Proc. of 1995/6 HERA Physics Workshop*, eds. G. Ingelman *et al.*, Vol. 1, p.23, arXiv:hep-ph/9609400.

[97] Z. Sullivan and P. M. Nadolsky, in *Proc. of the APS/DPF/DPB Summer Study on the Future of Particle Physics (Snowmass 2001)* ed. R. Davidson and C. Quigg, arXiv:hep-ph/0111358.

[98] B. W. Harris, E. Laenen, L. Phaf, Z. Sullivan, and S. Weinzierl, in preparation.

[99] S. D. Ellis and D. E. Soper, Phys. Rev. D **48**, 3160 (1993).